Low-Cost Sensors Provide Insight into Temporal Variation in Fugitive Methane Gas Concentrations Around an Energy Well

Neil A. Fleming*, Tiago A. Morais, M. Cathryn Ryan, Dep. of Geoscience, University of Calgary; *Corresponding author (naflemin@ucalgary.ca)

Keywords:

Gas migration, methane, well integrity, leak detection

Abstract

Effective measurement of the presence and rate of methane gas migration (GM) outside the casing of energy wells is important for managing social and environmental impacts and financial liabilities in the upstream petroleum industry. Practitioners typically assess GM by above-background methane gas concentrations in-soil or at-grade; however, factors influencing the potential variation in these measurements are not well represented in industry recommended best-practices.

Inexpensive chemoresistive sensors were used to record a one-minute frequency methane gas concentration time series over 19 days. Time series were recorded at three soil depths (0, 5, and 30 cm) at two locations <30m cm radially from a petroleum well with known GM, in addition to two 'control' locations. Observed concentration variations ranged over several orders of magnitude at all depths, with generally lower concentrations and more variation observed at shallower depths. Varying concentrations were correlated to meteorological factors, primarily including wind speed and shallow groundwater table elevation. The gas concentration patterns were affected by a 3.5 mm rainfall event, suggesting soil moisture changes affected preferential gas migration pathways. Results indicate potential variability in repeated snapshot GM test results. Although currently recommended GM detection methods would have effectively identified the presence/absence of GM, they would not have quantified order of magnitude changes in concentration. GM detection success at this site was increased with measurement at more than one location spatially within 30 cm of the well casing, lower concentration detection limits, and greater measurement depth. These findings indicate that meteorological factors should be considered when conducting gas migration surveys (particularly for improving at-grade test reliability). The low-cost approach for long-term concentration measurement facilitates insight into variable gas concentrations and may be advantageous in comparison to snapshot measurements in some circumstances.

Introduction

Well integrity failures, including Surface Casing Vent Flow (SCVF) and Gas Migration (GM) outside the outermost (or surface) casing, represent safety, environmental, and financial liabilities to the upstream oil and gas industry and negatively affect the oil and gas industry's social license (Dusseault et al. 2014; Cahill et al. 2017; Alboiu and Walker, 2019). Wells with SCVF or GM detected cannot be legally decommissioned in Canada, and therefore appropriate GM detection informs operational decision making on remedial cementing, with important environmental and social consequences, and financial implications (Trudel et al. 2019; Alberta Energy Regulator (AER) 2021; Schiffner et al. 2021). Decommissioning and reclamation costs for wells with SCVF or GM typically cost between $140K to $370K, with 5-10% of wells

costing considerably more (e.g., up to millions of dollars) due to SCVF/GM repair challenges (Trudel et al. 2019). These costs further increase if re-entry is required when SCVF/GM is discovered after a well has already been decommissioned (Dusseault et al. 2014; Trudel et al. 2019). Acute GM risk is primarily related to explosive hazard (between the lower and upper explosive limits of 5-15% methane v/v in a mixture with air) (Engelder, T. and Zevenbergen 2018; Molofsky et al. 2021). Therefore, accurately determining the potential for explosive combustible gas-air mixtures is central to classifying the risk of these wells (AER 2014; Molofsky et al. 2021). Importance thus needs to be placed on the detection and measurement approaches for SCVF and GM.

The most common detection method for SCVF is a simple 'bubble test', which determines if the vent flow will generate sufficient pressure to push a bubble through a 6-12 mm diameter tubing directed through a maximum backpressure of 2.5 cm water, within a ten-minute period (AER 2021). Alternate methods to the bubble test, including higher resolution and long-term remote monitoring, are applied commercially in situations benefiting from more definitive or continuous measurement, such as for accurate rate determination, tracking temporal trends, and observing SCVF response to remedial work (Dusseault and Jackson 2014).

Unlike SCVF measurement and monitoring, to our knowledge there are no commercially available approaches for continuous GM testing or monitoring. Commercial detection of the presence of GM outside the casing of energy wells is typically conducted through 'snapshot' GM detection surveys by sequentially measuring methane gas concentrations at numerous specified (and provider-dependent) soil depths and spacings around well-center. The test is comprised of multiple snapshot measurements over a short time period (i.e., less than one hour). Detection of above-background concentrations of 'combustible soil gas' (predominantly methane, along with trace amounts of other natural gas alkanes) indicates the presence of GM (Szatkowski et al. 2002). This approach was developed in the 1990's by an ad hoc industry group to assess presence or absence of GM and remains the recommended approach in Alberta (Abboud et al. 2020). In this approach, methane gas (hereafter referred to as 'gas') concentration is measured at a total of 14 test points: two within 30 cm of the well and then at 2, 4, and 6 m away (radially) orientated in a cross pattern (AER 2021). While not necessarily applied by practitioners, the regulators recommended equipment lower detection limit for this test is 1% of the methane Lower Explosive Limit (LEL, i.e., 500 ppm CH_4). Alternate testing spacings and depths, including at-grade measurement (as opposed to the AER-recommended 50 cm depth; Fleming et al. 2019), are applied by industry practitioners to minimize the added expense of auguring access holes, or sampling depths less than 30 cm to avoid requirements for ground disturbance permitting (e.g., Province of Alberta 2020; BC

Oil and Gas Activities Act 2020; Statutes of Saskatchewan 1998). These at-grade and relatively shallow sampling depths are permitted in regulation to encourage innovation and use of newly available technology (Natural Resources Canada, 2019; AER 2021).

The Alberta-recommended GM detection approach is largely duplicated or directly referenced in regulation across Canada (e.g., Government of Saskatchewan, 2015; OROGO, 2017; Pretch and Dempster, 2017; BCOGC, 2019). However, to our knowledge, there are no public reports demonstrating the advantage of subsurface detection strategies (e.g., up to 50 cm depth) or validating this approach in variable field conditions (Abboud et al. 2020). In addition, though it is anecdotally evident that these recommendations are not applied by all practitioners, there is little published information on the GM sampling and detection approach in GM testing reports (e.g., the AER 's Well Vent Flow/Gas Migration Report). Negative test results are also unavailable, leading to uncertainty in the total number of wells tested (Abboud et al. 2020; Sandl et al. 2021).

Temporally varying SCVF rates have been reported, indicating that long-term monitoring may be required to fully characterize emission rates and to ensure more reliable detection compared to short-term 'snapshot' measurements (Dusseault et al. 2014; Riddick et al. 2020). Previous researchers have also found soil-surface GM concentrations and effluxes to vary over hourly, daily, and seasonal scales (Forde et al. 2019b; Lyman et al. 2020). Spatiotemporal variation of CH_4 emissions and at-grade concentrations over time scales ranging from < 1 hour to daily scales has been further demonstrated by a two-week efflux experiments at six test points around a GM energy well in Eastern Alberta (Fleming et al. 2021). Historic GM survey test results at this well indicates variation between tests conducted by different parties, and by the same party on different occasions. This suggests a variation in measured concentrations due to both method-dependent mechanisms (e.g., testing depth and location), and method-independent temporal variations in the physical presence of combustible soil gases (Fleming et al. 2021, their Figure 2).

Temporal variation in gas concentrations and effluxes may be driven by episodic and pulsed movement of gas in the saturated zone (Cahill et al. 2017; Van de Ven et al. 2020) and due to changing atmospheric conditions (Kuang et al. 2013; Oliveira et al. 2018). Barometric pressure changes are also known to induce variable effluxes, and may cause atmospheric gases to flow into the soil during rising barometric pressures due to a pressure imbalance between atmospheric and soil gases (Abbas et al. 2010; Forde et al. 2019a). High wind speed has been shown to decrease measured at and above-grade methane concentrations from subsurface sources (Chamindu Deepagoda et al. 2016; Ulrich et al. 2019), and induce subsurface gas pressure variations that may drive higher effluxes and flush soil gases in the soil (Poulsen et al. 2017). Higher air temperatures may drive higher gas diffusion rates, while convective and buoyant

gas movement may be caused by differences in density due to temperature and the relative density of methane compared to air (Nachshon et al. 2011; Chamindu Deepagoda et al. 2016).

While these recoded variations in gas migration effluxes and concentrations may indicate relevant variations in measurable combustible gas concentrations, prior experiments have not explicitly demonstrated whether concentration variations, potentially driven by meteorological factors such as wind speed and atmospheric pressures and temperatures, occur in the subsurface in addition to the measured at-grade concentrations and effluxes. In addition, time series measurements simultaneously at multiple depths were not possible using a single high-resolution gas analyzer connected to multiplexed flux chambers in previous studies (e.g., Forde et al. 2019b; Fleming et al. 2021). While previous studies of gas migration efflux are relevant from a methane emissions measurement perspective (Forde et al. 2019b; Lyman et al. 2020; Fleming et al. 2021) and effluxes may be used to detect GM (Forde et al. 2019b; Schout et al. 2019), most practitioners currently rely on concentration measurement. Thus, understanding methane concentration variability is more applicable to the current practice in GM detection. To the authors knowledge, previously published work has not recorded temporal variation of in-soil fugitive gas concentrations at a high resolution over multiple days, nor analyzed how this variation may affect the successful detection of wells with GM.

Here we use inexpensive chemoresistive sensors to record a high-frequency combustible gas concentration time series at multiple depths around a case study well with GM. With the aim of improving GM testing and monitoring practices, this field experiment specifically sought to evaluate whether:

- Measurable methane concentrations are higher at greater depths in the soil.
- Measurable methane concentrations are temporally variable both at-grade and at depth into the soil.
- If present, these variations in measurable methane concentration coincide with varying meteorological conditions such as precipitation, wind speed and barometric pressure changes.

Materials and Methods

Study well description.

Field access to a suspended petroleum production well with GM was provided by an anonymous industry partner. Previous site investigations confirmed the presence of detectable GM focused outside the well casing, with estimated average emissions within a 25 cm radius around the well-center of 0.3 m^3 CH_4 d^{-1} (130 g d^{-1}) and no detectable SCVF (Fleming et al. 2021). Gas concentrations in 14 different detection surveys conducted over > 10 years document a consistently detectable presence of GM focused

near the well casing, though the maximum measured concentrations during commercial GM testing have varied from <100 to 110,000 ppm. In each survey, the highest methane gas concentrations were observed near the well casing (i.e., the two measurements spatially located "within 30 cm of wellbore on opposite sides": AER 2021). This spatial distribution is common in most GM surveys (Erno and Schmitz 1996; Lyman et al. 2020) with some exceptions (Forde et al. 2019b).

Soil gas sampled immediately against the outer casing at 30 cm depth yielded thermogenic methane concentrations as high as 87% gas by volume with minor concentrations of higher alkanes, consistent with common GM composition (Fleming et al. 2021). Compositional analyses of the 61 soil gas samples (sampled by the authors at depths from 0 to 30 cm within 1.5 m of the well) include a mean and maximum concentration of C2+ gas concentrations (including ethane [C2], propane [C3], nC4, iC4, neopentane, iC5, nC5, and nC6) of 0.069 % v/v and 0.378 % v/v, respectively. The mean methane [C1] concentration for the same sample set was 18.4 % v/v, indicating that the combustible soil gases were predominantly (i.e., > 97 % v/v) methane. The balance of average soil gas compositions (in order of decreasing mean abundance) were N_2 (64.5%), O_2 (14.4%), CO_2 (1.4 %), and Ar (0.74%). Atmospheric methane concentrations sampled five meters South of the well in October 2019 averaged 2.5 ppm (max 5.5 ppm) (Fleming et al. 2021). The shallow lithology, as observed by hand auger samples, is fine silty sand down at least 2 meters, with a water table ~ 0.5 m below ground surface. The prevailing wind direction in the region is westerly (Alberta Agriculture and Forestry, 2020).

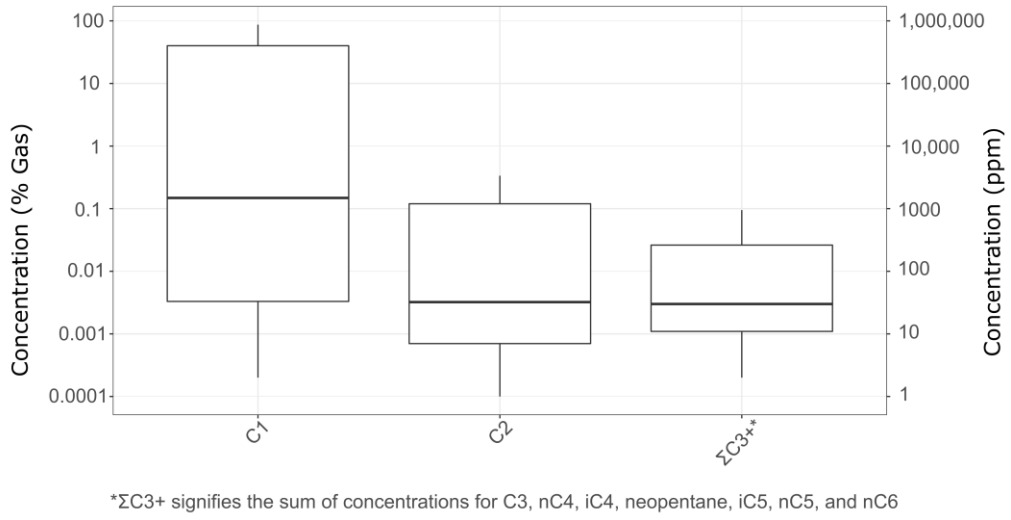

Fig. 1—Boxplot showing the relative occurrence of C1 (methane), C2 (ethane), and C3+ in combustible soil gas compositions. The boxplots include analyses from 61 samples collected at 0-30 cm depth and < 1.5 meters radius from the study well. The logarithmic vertical axes show percent composition (left axis)

and ppm (right axis). The boxplot graphically illustrates the minimum, 1st quartile, median, 3rd quartile, and maximum measured concentrations.

Sensor measurement of methane concentration.

Sensors were installed at four locations to monitor methane gas concentrations at one-minute frequency over 19 days (October 3-22, 2020). Chemoresistive MQ-4 combustible gas sensors with high sensitivity to methane (Henan Hanwei Electronics Co. Ltd.) were inserted into water-resistant housings **(Fig A-1).** Sensor loop resistances were recorded at one-minute frequency on a datalogger (CR1000, Campbell Scientific). Since the dominant form (> 97%) of combustible gas in GM at this site is methane **(Fig. 1)**, the term gas concentrations is used to represent methane concentration herein. Two vertical sensor nests, which included sensors at depths of 0 (i.e., at-grade), 0.05, and 0.30 meters below ground surface, were located five centimeters radially from the East and West sides of the surface casing (**Fig. 2**; Fig A-1). Two distal (i.e., 'control' to the GM around the well casing) sensors located 5 m to the East of the surface casing, were installed at 0.05 m depth to document sensor noise and any response that could be caused by variable temperature and humidity factors. Of the two distal sensors, one was installed in native soil at 0.05 m depth (referred to as the distal 'soil baseline' sensor). The second was isolated from subsurface methane gas efflux by installation at 0.05 m depth in moist filter sand inside an open-topped polyethylene container (0.3 m diameter by 0.3 m depth) that was buried in the soil, with the sand filled to grade (referred to as the distal 'isolated' sensor).

The location of the sensor nests near the well was chosen to represent typical testing practices for measurements nearest the well, with two measurements within 30 cm of the well on opposite sides (e.g., AER 2021). The chosen depths were based on anecdotal information around the common measurement depths employed by service companies that conduct gas migration testing around energy wells. As previously mentioned, the 30 cm threshold is commonly used because depths less than this do not typically require ground disturbance permitting (e.g., Province of Alberta 2020; BC Oil and Gas Activities Act 2020; Statutes of Saskatchewan 1998).

The MQ-4 sensors use a tin dioxide (SnO_2) chemoresistive semiconductor which is responsive to combustible gases, including methane (CH_4) and other light hydrocarbon gases present from gas migration (Honeycutt et al. 2019). The sensor resistance is constant in the presence of clean air (i.e., mostly N_2 and O_2, with negligible CH_4 concentrations; Henan Hanwei Electronics Co. Ltd.). A passive diffusive sampling method is used to deliver target gases to the sensor, where hydrocarbon gases react with available oxygen causing a non-linear decrease in sensing loop resistance with increasing hydrocarbon

gas concentration (Honeycutt et al., 2019). These sensors are reactive in the presence of any light hydrocarbon gas, including other alkanes (C2+), but are most sensitive to CH_4 (Henan Hanwei Electronics Co. Ltd.). Previous experiments on sensors using a similar principle of measurement indicate limited interference by CO_2 (Sekhar et al. 2016). The sensors are also slightly impacted by variable humidity and temperature (Henan Hanwei Electronics Co. Ltd.). These inexpensive sensors (~CAN $5 per unit) have been previously suggested or used for similar applications, including natural gas leak detection (Mitton, 2018), and continuous efflux measurements around wellheads (Riddick et al. 2020).

Sensor-specific exponential calibration curves between methane concentration and raw voltage response were developed in the laboratory. While these sensors are responsive to a range of combustible hydrocarbon gases, calibration and reporting as ppm methane is justified by the relatively minor presence (< 3%) of C2+ gases in comparison to methane (Fig. 1). Manufacturer response curves indicate that low C2+ gas concentrations would induce a similar response to an equivalent concentration where CH_4 is the only alkane present (Henan Hanwei Electronics Co. Ltd.). Previous gas composition data (Fig. 1) indicate that methane concentrations over the measurement period may have infrequently exceeded the manufacturer recommended 5% methane by volume, potentially leading to an underestimate of true methane concentrations above this 5% threshold. Detailed sensor validation and calibration methods, in addition to details on the solar power supply and field installation, are described in Appendices A through C.

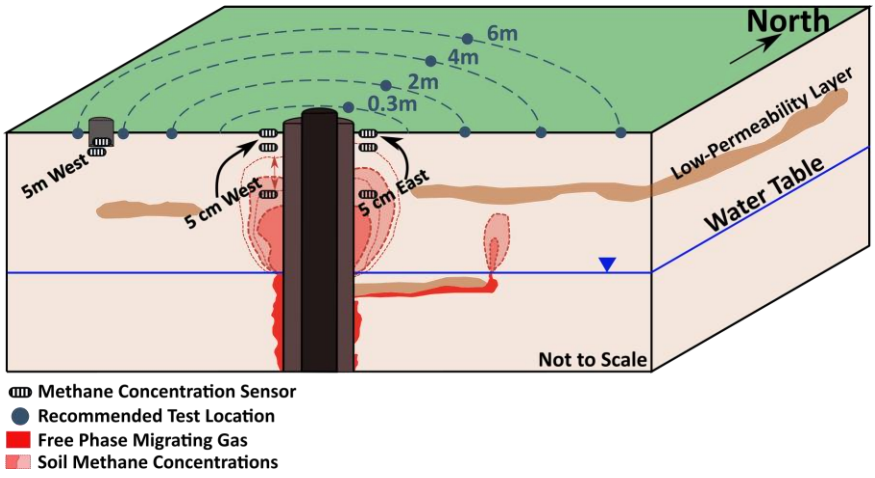

Fig. 2— Case study site cross section conceptual diagram showing the methane migration along the wellbore and underneath a low-permeability layer (After Forde et al. 2019b). Methane concentration sensors are 5 cm from the well casing on the East and West sides, at depths of 30, 5, and 0 cm. Two additional sensors are 5 m West in-soil and in an isolated enclosure. Recommended test locations for Western Canadian gas migration detection are shown as points.

Meteorological data collection during monitoring period.

Precipitation and wind speed data were retrieved from the nearest public weather station (10-20 km away) (Alberta Agriculture and Forestry, 2020) for the monitoring period. Water levels from a hand-installed piezometer (screen centered 1.0 m depth below ground surface, 1.25 m South of well-center) and on-site atmospheric temperature and pressure were recorded hourly (Levelogger®). The water levels were barometrically compensated with a Barologger®. Water level and barometric pressure change rates were approximated as a five-hour central difference, which was the shortest time interval that returned a visually smooth change rate.

Data processing.

Sensor response data were processed in R (R Core Team 2020), where the calibration curves were used to convert raw voltage to methane gas concentrations before being compared to meteorological and site conditions. Data analyses included Pearson correlation analyses between gas concentrations and meteorological factors (including wind speed, temperature, barometric pressure and pressure change), and groundwater level and water level change. Short-term (i.e., hourly and daily) and full-period (19 day) variation in concentrations by depth and location were assessed visually and by comparing the coefficient of variation (normalized standard deviation) of different sensors (Appendix C). As a proxy for industry-performed snapshot measurement, the single and dual-point detection success rate was assessed over working hours (07:00 – 18:00). The calculated success rate was the percentage of one-minute frequency measurements that were detected above a range of concentration thresholds (2, 25, 50, 100, 500, 1000, 5000, and 10 000 ppm) at each depth. Dual-point analyses considered both sensors at a given depth (at-grade, 5, or 30 cm) to represent typical testing practices with two measurements within 30 cm of the well, while the single-point analysis presents the results from only one sensor. The detection success rate indicates the percentage of measurement occasions where individual snapshot concentration measurements, or the combination of two snapshot measurements at the same depth, would correctly indicate the presence of GM or potential concentration exceedances. Different concentration thresholds represent different portable measurement equipment with a range of detection limits, and variations in operator decision making (e.g., attributing any concentration below a certain limit to be a non-definitive GM signal).

Results and Discussion

Meteorological conditions over the monitoring period.

The equipment was deployed, and monitoring data collected over a 19-day period (3-22 October 2020). Diurnally varying on-site air temperature was superimposed on a steadily temperature decline over the monitoring period, with freezing temperatures overnight first observed on the fifth night (October 7th) that were sustained after October 12th (**Fig. 3**). Air temperatures ranged from 10 ℃ to below -14.5 ℃, leading to soil frost (observed to two cm depth by the end of monitoring). Barometrically compensated groundwater levels were moderately variable on daily time scales and showed a sharp response (> 30 cm rise) to a cumulative 3.5 mm precipitation event on October 11th (Fig. 3). More moderate precipitation events that occurred several days did not show marked water level changes. Wind speeds also demonstrated a quasi-diurnal fluctuation with generally higher wind speeds in the daytime.

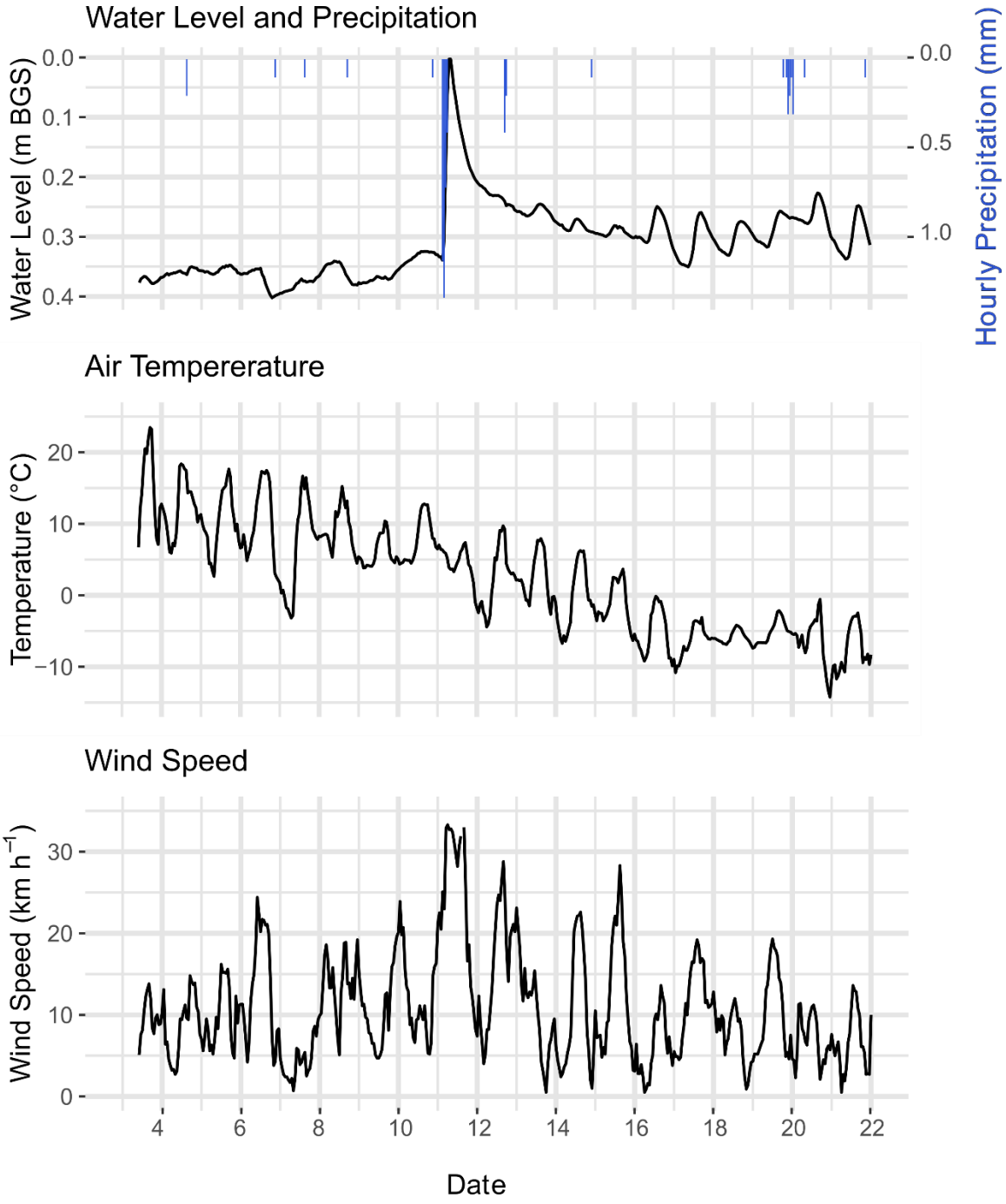

257

258 **Fig. 3—**Water level in meters below ground surface (m below ground surface), and selected
259 meteorological data from the nearest public weather station, including hourly precipitation (mm), air
260 temperature (℃), and wind speed (km h^{-1}) over the monitoring period. The vertical bars indicate midnight
261 of the October 2020 calendar date indicated.

262

Time series methane concentrations response.

The sensors in the two sensor nests near the well recorded temporally variable methane concentrations in the soil and at-grade with the soil surface. Methane concentrations tended to be higher at greater depth (**Fig. 4**), with mean hourly concentrations combined from both (East and West) nests of 8,500, 11,500, and 25,200 ppm at the 0, 5 and 30 cm depths, respectively. Methane concentrations ranged from <2 ppm to ≥ 50 000 ppm (i.e., 5% of gas composition). Ten mean hourly methane concentration values measured at the West 30 cm depth sensor exceeded the 5% gas manufacturer recommended detection range. Less than 0.1% of one-minute measured concentrations were below 2 ppm (**Table 2**).

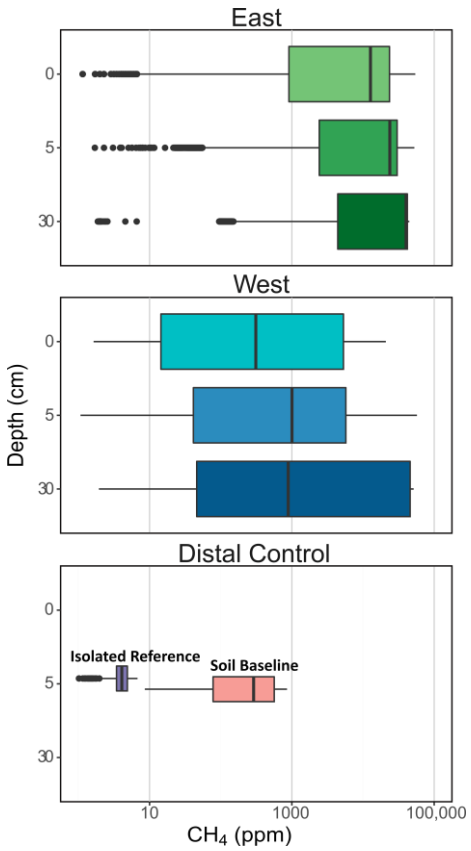

Fig. 4—One-minute frequency soil methane concentration boxplots (log ppm CH_4) plotted with depth and separated by sensor array location (East, West and Distal Control) over the full 19-day measurement series. Box and whiskers indicate minimum, 1st quartile, median (vertical line), 3rd quartile, and maximum concentrations, with 'outliers' exceeding 1.5 times the interquartile range below the 1st quartile represented as points.

The distal sensors recorded relatively low methane concentrations with moderate variability over the monitoring period (**Fig. D-1**), and generally lower amounts of variation in comparison to the sensors

in the nests near the well (**Table C-1**). Both distal sensors had limited diurnal fluctuations with slightly higher concentrations observed during the daytime. Diurnal variation may be partly explained by the influence of temperature and humidity on the sensors. In future studies, the influence of temperature and humidity should be more robustly assessed. The distal 'soil baseline' sensor recorded a steadily declining concentration over the time series between a maximum of 840 ppm at the start of the testing period to a minimum of 40 ppm, while the 'isolated reference' sensor steadily fluctuated between 0-10 ppm over the full measurement period (**Fig. 5**). The higher methane concentrations recorded by the 'soil baseline' sensor may indicate a moderate subsurface GM signature at a 5 m distance from the well. The modest fluctuation between expected atmospheric concentrations for the 'isolated reference' sensor, with no apparent impact from precipitation or freezing air temperatures, indicates that the sensor performance was not significantly affected by these factors. The calibrated concentrations are largely within expected methane concentrations for all sensors based on expected atmospheric concentrations (~2 ppm) and previously measured soil gas concentrations, though the calibration method and sensor detection limits may have led to an underestimate of true methane concentrations which exceeded 5% gas.

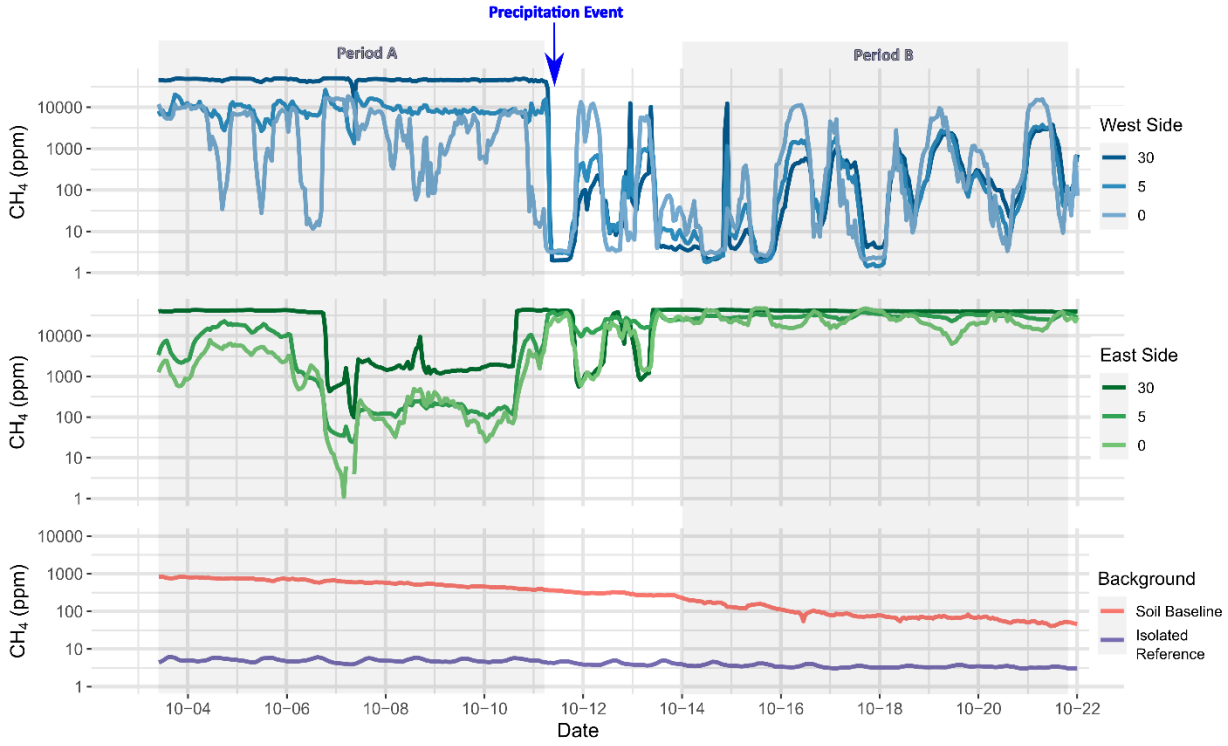

Fig. 5—Time series of hourly averaged methane concentrations (ppm) around an energy well with gas migration observed between October 3-22, 2020. Sensors were deployed in two arrays (located at 5 cm distance of the energy well casing on each of the East and West sides) at three depths (0, 5, and 30 cm).

Additional 'control' sensors were located 5 m distance from the energy well on the east side as a 'baseline' 5 cm in-soil methane concentration (Orange), and an 'isolated reference' sensor placed at 5 cm depth and protected from soil gases in an enclosure (Purple). Period A and B (shaded) correspond to analysis periods with visually regular concentration variations prior to (Period A), and following a three-day lag after a 3.5 mm precipitation event (Period B). The vertical log scale and decreasing sensitivity approaching the sensor detection limit (5% gas; 50 000 ppm) may contribute to the apparently lower variability at high concentrations.

Change in observed distribution of methane concentrations and implications in gas movement behavior associated with a precipitation event.

An observed change in methane concentrations, and concentration variation behavior, coinciding with a minor 3.5 mm precipitation event on October 11th (Fig. 3) prompted separation of the analysis into two periods preceding and following a three-day lag after the 3.5 mm precipitation event (**Fig. D-2**). There are relatively distinct methane concentration profile time series in each period (Fig. 5). Methane concentrations in the Western array sensors were higher and more consistent prior to the October 11th precipitation event, and showed a more pronounced daily-scale variation over several orders of magnitude after the precipitation event. Conversely, the Eastern array sensors had higher concentrations beginning on October 13th, with a lower amount of daily variation. Differences between the two arrays before and after the precipitation event (Period A and B in Fig. 5) was also evident in different correlations with meteorological factors for the two analysis periods (**Table 1)**. The 5 m distal 'soil baseline' and 'isolated reference' sensors concentrations were not visually different following the precipitation event. There were also no substantially different correlations with meteorological factors between the two periods for the reference and baseline sensors, indicating that the precipitation event may not have impacted these measurements.

The precipitation event caused a significant water table rise (~0.33 m; Fig. 3), with associated changes in the soil moisture content distribution, both of which would have altered the effective gas permeability of the soil around the well. Previous observations of soil gas concentrations and effluxes at this well (Fleming et al. 2021), and by researchers in other settings (Chamindo Deepagoda et al. 2018) suggest that gas movement from the water table to ground surface occurs through preferential flow pathways. The precipitation event and associated change in water level and soil moisture content may have induced a change in the advective movement of gas in the soil around the well casing by occupying

pore spaces with water. This would have thereby changed the preferential movement pathway of gas within the saturated and unsaturated zone and lead to a shift in the gas concentration distribution.

Temporal variability patterns as a function of depth and location.

While measured concentrations at all depths varied by several orders of magnitude over the 19-day time series, concentrations were generally higher at greater depths in the soil (Fig. 4). This concentration distribution is expected given the tendency of saturated zone gas migration to occur in relatively narrow, discrete zones focused around the well casing (Erno and Schmitz, 1996; Dusseault et al. 2014; Lyman et al. 2020; Van de Ven et al. 2020) combined with the shallow water table at the site. The methane gas exits the water table at discrete locations, and once in the unsaturated zone it will disperse radially and vertically by soil gas advection and diffusion (Figure 2; Chamindu Deepagoda et al. 2016; Forde et al. 2018). Given the shallow water table, there is relatively little opportunity for radial dispersion.

Temporal variability in measured concentrations were substantially greater in sensors near the energy well (compared to the distal sensors) at short-term (e.g., several minutes), hourly and daily scales. The coefficient of variation (i.e., the measurement variation as a percentage of the mean) was generally higher for sensors closer to the surface (Table C-1), and the increasingly pronounced variation at shallower depths is visible in the short-term time series showing one-minute frequency measurements (**Fig. 6**). For comparison to variability at other sensors, see the laboratory baseline noise test (**Fig. C-2**) and field observations of one-minute frequency variability at the five-meter distal location (**Fig. D-1**).

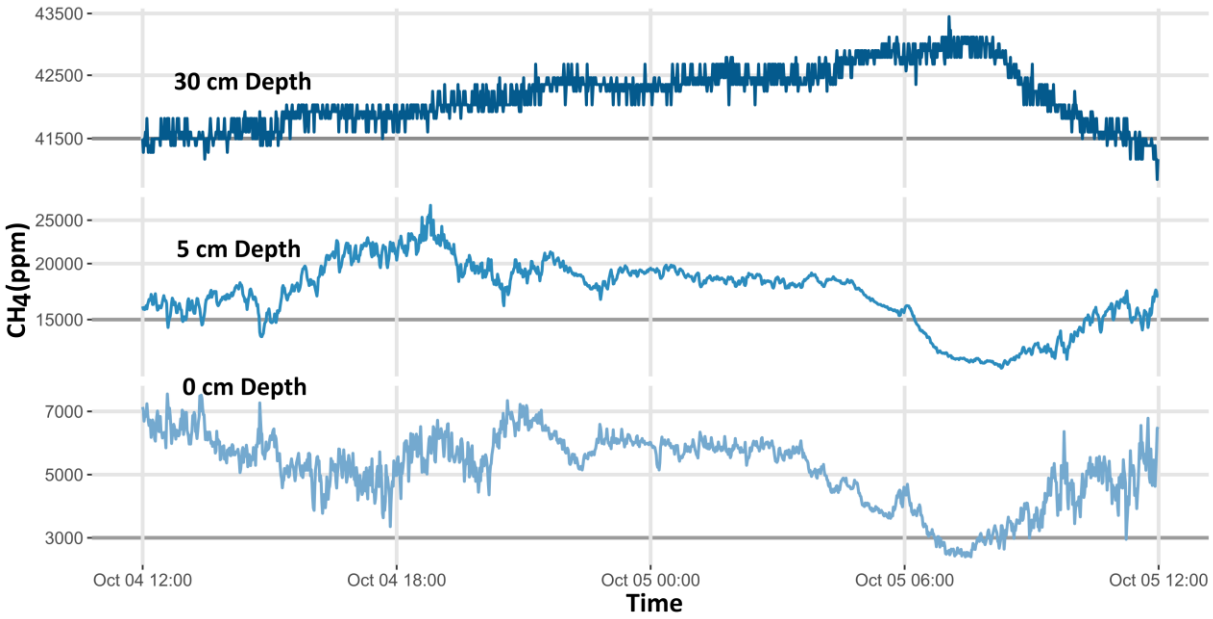

Fig. 6—Methane concentration (ppm) time series plotted with one-minute measurement frequency over 24 hours for three depths 5 cm from the East side of the casing of an energy well with gas migration. Note the different y axes scales for methane concentration at the three depths.

Temporal variability at all depths may be explained by a combination of i) variations in methane transport and arrival at the water table; and ii) changing rates of advective gas movement in the soil zone causing varied gas exchange and mixing with the atmosphere across the ground surface interface. In the first instance, the complex interaction between buoyancy and capillary forces in a heterogeneous porous media are expected to result in temporally variable and continuous or discontinuous changes in gas movement pathways and transport rates through the saturated zone (Gorody 2012; Van de Ven et al. 2020). Episodic arrivals of migrating gases driven by ebullition events in the saturated zone will induce short-term changes in soil gas concentrations (Forde et al. 2019b). In the second instance, variable soil gas movement pathways, efflux rates, and mixing with atmospheric gases may be caused by varying meteorological conditions (e.g., barometric pressure, wind, temperature) in addition to soil moisture and groundwater levels (Nachshon et al. 2011; Chamindu Deepagoda et al. 2016). Short-term air pressure fluctuations induced by wind may have caused the observed depth-dependent variation in concentrations at the minute-scale (Fig. 6; Table C-1) (Poulsen et al. 2017).

Methane concentration correlation to meteorological factors.

Simple regression analyses assessed the correlation between hourly averaged soil gas concentrations and meteorological and site factors including atmospheric pressures, temperature, and wind speed, and water level in a shallow piezometer (Fig. D-2, **Fig. D-3**). Given the inherent autocorrelation between meteorological factors (for example, both atmospheric temperatures and wind speeds typically fluctuate diurnally), some of these observed correlations may be spurious.

	Before Precipitation Event (Period A)					After Precipitation Event (Period B)				
Sensor Depth (cm)	U_wind	P_{ATM}	T_air	WL	dP_{ATM}/dt	U_wind	P_{ATM}	T_air	WL	dP_{ATM}/dt
West Sensors (windward side)										
0	**-0.68**	0.31	-0.32	0.39	0.03	-0.33	-0.14	-0.29	0.11	-0.26
5	-0.32	0.25	0.08	0.34	0.06	-0.15	0.30	-0.30	0.39	0.05
30	-0.29	0.01	-0.02	0.10	0.03	-0.11	0.31	-0.25	0.36	0.10
East Sensors (leeward side)										
0	0.02	-0.04	0.35	-0.25	0.23	0.24	*0.45*	0.11	0.15	0.19
5	-0.05	-0.02	0.30	-0.25	0.17	0.04	0.41	-0.06	0.12	-0.08
30	0.11	-0.10	*0.45*	-0.26	0.14	-0.23	*0.53*	-0.28	*0.49*	-0.01
Isolated Reference Sensor (5m distance from well)										
5	0.27	-0.19	**0.90**	-0.26	-0.14	*0.55*	**-0.72**	**0.94**	**-0.64**	-0.07
Soil Baseline Sensor (5m distance from well)										
5	-0.27	0.58	0.30	0.34	0.13	0.39	**-0.82**	**0.75**	**-0.66**	0.07

Table 1—Pearson correlation coefficients (r) between methane concentrations at each sensor (where the proximal arrays labelled as West or East of energy well, and depth in cm) and relevant meteorological factors for data periods before and after the rainfall period event (Periods A and B, Fig. 5). Meteorological factors include wind speed (U_wind), barometric pressure (P_{ATM}), atmospheric temperature (T_air), piezometer water level (WL), and barometric pressure change (dP_{ATM}/dt). Pearson coefficients greater than 0.45 are italicized, while those greater than 0.6 are bolded.

A negative correlation was observed with wind speed in the array on the upwind (West) side of the well (e.g., Pearson r = -0.68 and -0.33 in Period's A and B, respectively in the at-grade sensor), with higher soil gas concentrations are observed during times of lower wind speeds. This negative correlation was absent for the leeward (East) side sensors (**Table 1**). Decreasing correlation strength with depth suggests the wind effect decreases with depth. The impact of wind on soil gas movement is well supported, since wind causes moderate pressure variations at ground surface, leading to pressure pumping and an increased gas exchange between the soil and atmosphere (Redeker et al. 2015; Poulsen

et al. 2017). Near the soil surface, wind may also cause methane transport laterally downwind from preferential efflux pathways (Chamindu Deepagoda et al. 2018). This may potentially explain the negative correlation with wind on the West sensors (upwind of the inferred preferential gas movement pathway along the casing for the predominant wind direction) and a slight positive correlation to the East (generally downwind).

Barometric pressure change has previously been shown to induce exchange between soil and atmospheric gases due to a pressure differential between the atmosphere and soil gases (Börjesson and Svensson 1997; Forde et al. 2019a). This study showed an inconsistent and low correlation (up to -0.26 at the at-grade West sensor; Table 1) for the atmospheric pressure change rate, dP_{ATM}/dt. Rising barometric pressure is expected to cause atmospheric gases to be pushed into the upper soil zone and therefore a decrease methane concentration (Abbas et al. 2010). This effect may be stronger in regions with thicker unsaturated zones (Forde et al. 2019a).

Changes in water level can affect soil gas transport pathways and effective gas conductivity as moisture contents change (Chamindu Deepagoda et al. 2018) and/or induce advective gas movement (Fuki, 1987; Abbas 2011), or due to changes in preferential methane transport pathways in the saturated zone. Low correlation coefficients were seen with water level that were variably positive (West sensors; Table 1) or negative (East Sensors in Period A; Table 1).

A moderate correlation with atmospheric temperature, particularly for the sensors in the Eastern array, may be explained by changes in buoyancy-driven flow and higher diffusion rates at higher temperatures (Nachshon et al. 2011; Chamindu Deepagoda et al. 2016). Increased soil temperature is also related to higher microbial methane oxidation rates (Stein and Hettiaratchi 2001). However, the magnitude of expected daily temperature variation was previously found to be too small to produce daily-scale changes in methane efflux attributable to methane oxidation variation at this site (Fleming et al. 2021). The distal reference sensors 5 m to the West (typically upwind from the well) were used to compare sensor output concentrations that may be attributed to changes in soil temperatures and relative humidity, and atmospheric methane concentrations. The isolated reference sensor showed a very strong positive correlation between atmospheric temperature and concentration, resulting in a daily cycle between 3 and 6 ppm with daily maxima occurring in early afternoon. This indicates the magnitude of variation that might be expected at the 5 cm depth due to changes in soil temperature and humidity (thereby impacting sensor response in ways not related to soil gas concentrations). This variation may also be caused by daily cycles in atmospheric methane mixing ratios (Simpson et al. 1999). Concentrations in the soil baseline sensor also exhibited a moderate daily cycle superimposed on a progressive decline

between 840 to <100 ppm CH4, the cause of which is not clear. Visual comparison and the correlation coefficients both suggest that the soil baseline sensor response was most strongly related to atmospheric temperature, with weaker (and potentially spurious) relationships to wind speed and water levels.

In summary, the measured soil gas concentrations near the well casing are correlated to several meteorological factors that may partially explain some of the observed concentration variation. The distal reference sensors fluctuate regularly and indicate a small amount of variation, contrasting the pronounced variations observed on the minute, hourly, and daily time scales near the zones of highest methane migration efflux. While several factors were strongly correlated to measured concentrations at particular sensors (most notably wind speed at the Western (windward) array during the pre-precipitation analysis period), no clear patterns were observed for all sensors, or prior to vs. after the precipitation event.

Revisiting the objectives posed in the introduction, it is observed that gas concentrations were generally higher at greater depths, though all sensors varied temporally over multiple orders of magnitude, and occasionally reversals of the methane concentration gradient were observed. The methane concentrations were highly temporally variable and sometimes correlated to wind speed, temperature, and barometric pressure. The complex interaction between these multiple factors and the spatially variable soil migration zone clearly precludes generalization of these effects based on this short time series at a single field site. Confidence in these findings will be increased through additional studies at other field settings with different surface conditions (such as soil type, and vadose zone thickness), and well-specific factors such as gas migration rates, well configuration, and local geology. Commercial and scientific viability of long-term methane concentration measurements will be affected by repeated site access constraints to deploy and collect the equipment, and equipment constraints such as power supply and data logging.

Implications for gas migration detection and risk assessment.

This high frequency methane gas concentrations time series around an energy well with GM has important implications for the GM detection and risk assessment using concentration-based measurements. Variations in methane concentrations within proximity of the well casing at all measured depths indicate the potential variability in repeated snapshot GM tests. Considering the magnitude of potential temporal variability at hourly and daily scales, snapshot, or even repeated snapshot, methane concentrations measurements may falsely indicate trends in measured concentration or underestimate potential concentration-based risk exceedances (e.g., explosive limits).

Methane gas concentrations changed spatially between the two arrays and with depth over several time scales. Surface concentrations at the two arrays, both within 5 cm of the well casing, varied over multiple orders of magnitude between > 10 000 ppm (1 % gas v/v) to < 100 ppm over the 19-day measurement period (Fig. 5). The magnitude of relative variability and correlation between meteorological factors such as wind speed was generally greater at shallower depths. Results support previous findings that at-grade measurements are particularly susceptible to impacts from variable meteorological factors (Chamindu Deepagoda et al. 2016; Fleming et al. 2021).

Sensor Depth (cm)	Methane Analysis Detection Limit (ppm)							
	2	25	50	100	**500**	1000	5000	*10 000*
	Detection Success rate (%) for Individual Sensors							
	West Sensors (Upwind)							
0	99.8	60.6	55.5	50.3	39.7	35.4	20.1	6.1
5	95.6	74.6	69.0	66.1	57.3	51.0	23.9	12.4
30	98.3	77.7	73.2	69.6	56.3	51.1	43.0	42.9
	East Sensors (Leeward)							
0	98.8	98.0	97.9	92.1	79.4	76.1	60.2	52.3
5	99.9	98.7	97.9	97.7	79.6	76.2	71.5	69.2
30	99.8	99.6	99.6	99.2	98.0	97.9	77.5	76.7
	Detection Success (%) for Two Sensors (East and West) at the Same Depth							
0	99.9	99.7	99.7	99.6	97.3	93.4	75.5	55.7
5	99.9	99.7	99.6	99.6	99.6	97.7	87.5	79.0
30	99.9	99.6	99.6	99.6	99.6	99.6	96.3	96.0

Table 2—Detection success rate (% of measurements that would have been above a given detection limit lower cut-off), for one-minute-frequency daytime measurements during working hours (07:00 to 18:00) over 19 days. Two-sensor success indicates the success rate where either or both sensors at each depth exceed the concentration cut-off. The recommended detection limit, 500 ppm (i.e., 1% of the Lower Explosive Limit, LEL) is bolded (AER 2021). The 10 000 ppm (i.e., 20% LEL, 1% methane v/v) limit requiring immediate action and restricted worksite access is italicized (Occupational Health and Safety Code; Molofsky et al. 2021).

One-minute frequency measurements were below the expected atmospheric concentration (~2 ppm) in 4.4 to 0.1% of measurements, indicating the frequency of potential range issues with these sensors and the calibration method used (Table 2). The chances of detecting GM at a 500 ppm cut-off during working hours using at-grade single-point measurement was 39.7% and 79.4 % for the West and East 0 cm sensors, respectively. Both single-point and dual-point measurement detection success rates

were generally higher at greater depths and declined with higher concentration cut-offs (Table 2). Dual-sensor detection success was greater than single-point detector success, though 2.7% of at-grade dual-sensor measurements did not exceed 500 ppm.

At-grade concentrations were only marginally detectable for single-point measurements during some periods of the 19-day monitoring record, indicating lower detection success for at-grade measurements when using a single point (Table 2; Schout et al. 2019). When both measurement points were considered at each depth (i.e., two measurement points within 30 cm of the wellbore, as currently recommended in Alberta; AER 2021), the detection success rate was substantially higher (i.e., > 97.3 % when the recommended detection limits (500 pm) is used; Table 2). This indicates the tendency for increasing testing success with higher spatial measurement density, especially near the well. When detection limits were < 500 ppm, greater measurement depth did not substantially improve two-sensor detection success. These results indicate that shallower measurements using lower sensitivity detectors (e.g., 500 ppm, or 1% LEL, detection limit) have a lower chance of detecting above-background gas concentrations indicative of GM in comparison to deeper measurements or measurements made with more sensitive instruments.

Gas concentrations were generally higher at greater depths; however, their temporal fluctuations indicates that even subsurface measurements may need to consider temporal variability and meteorological influences. The advantages of higher subsurface methane concentration measurements were obtained without exceeding the 30 cm depth ground disturbance threshold, and greater detection success was obtained through two at-grade test points instead of a single test point at greater depth. The use of lower detection limits (< 100 ppm) with two at-grade measurements, obviated the advantage to subsurface measurement at this site. Increased confidence in GM test results may be obtained by using higher sensitivity detectors, measuring at greater depths in soil or at higher spatial density, and by withholding GM testing during periods of inappropriate meteorological conditions such as high wind speeds, barometric pressure increases, or following precipitation events.

This study has demonstrated the feasibility of installing inexpensive long-term sensors at-grade with the soil-surface, or in the shallow soil zone, as an alternative method to detecting and monitoring the presence of GM, in a manner that is resilient to temporal variability. Considering the financial, social, and environmental liability implications, accurate GM testing may be particularly relevant in higher risk areas such as where urbanization is encroaching on legacy oil/gas infrastructure (Gurevich et al. 1993; AER 2014; Abboud et al. 2020).

Variable concentrations observed at-grade can potentially introducing error into risk assessments based on snapshot concentration measurements. In comparison to the relatively reliable GM detection using two-sensor snapshot measurements during this case-study, 44% of at-grade measurements (and 4% of 30 cm depth measurements) would have failed to recognize the capacity for gas concentrations around this case-study well to occasionally exceed 10 000 ppm (Table 2). In outdoor spaces, elevated methane concentrations at-grade or within the soil are expected to rapidly decrease to low (non-explosive) concentrations upon mixing in the atmosphere above the well (Ulrich et al. 2019). However, these data show that testing conducted at certain times may underestimate the maximum potential concentrations. Improved confidence in these GM risk assessments will be obtained with long-term measurement, especially over periods that might be expected to result in higher at-grade gas concentrations (such as lower wind speeds). Accurate long-term concentration data can also be used to guide site-specific mitigation and management options.

Decreasing detection limits in gas measurement equipment (e.g., high-precision optical absorption gas sensors) and refinements to GM testing techniques inevitably leads to increased detectability of lower methane concentrations. This makes it increasingly difficult to meet the requirement to repair wells to a state of non-detectable gas migration in Alberta (AER 2021). Existing and historically available technologies and methods already detect the higher concentrations which are associated with higher rates of leakage (Erno and Schmitz 1996; Forde et al. 2018; Fleming et al. 2021). In essence, improved GM detection will increase the total number of wells classified with GM, with most of them in the 'low-rate' GM category (e.g., efflux of < 1 m^3 CH_4 day^{-1}).

The challenge and expense in well repair has led to a disproportionate number of wells that are idle (i.e., with suspended status in Alberta) (Muehlenbachs, 2017; Schiffner et al. 2021). Incorporating the 'social cost' of methane emissions may economically incentivize the repair and decommissioning of wells with higher emissions (e.g., 43 m^3 day^{-1} considering both GM and SCVF; Schiffner et al. 2021). However, the 'low-leaker' wells (like the well presented here; Fleming et al. 2021) are anecdotally the most difficult to repair. They are consequently the largest fraction of idle wells, which contribute to insolvency in the energy industry (Schiffner et al. 2021). Emission distributions suggest that the average GM and SCVF rates are heavily influenced by a small number of 'super-emitter' wells which contribute disproportionately to the overall leakage volumes (Erno and Schmitz 1996; Brandt et al. 2014; Kang et al. 2014; Zavala-Araiza et al. 2015; Saint-Vincent et al. 2020). From a methane emissions perspective, the detection and repair of these 'super emitter' wells will contribute the most to decreasing total emissions from GM sources. In contrast, at many well pads the contribution of methane emissions through low-rate GM may be

insubstantial in the larger perspective of all emissions at the well pad scale, and more broadly within the upstream oil and gas industry (Lyman et al. 2020). Given the conundrum presented by improved GM detection and investigation, with decreasing returns on emissions reduction through the repair of 'low-leaker' wells, it may be prudent for regulators to consider adopting a non-zero permissible GM rate (Natural Resources Canada, 2019). In this case, regulators could permit well decommissioning with low, but acceptable, methane emissions or risk classification (Dusseault et al. 2014; Natural Resources Canada 2019).

We have shown that point measurements may be insufficient to assess methane concentration-based risk, and it is known that emission rates of both GM and SCVF can be variable over time, requiring long-term measurement for accurate assessment (Lyman et al. 2020; Riddick et al. 2020; Fleming et al. 2021). Longer term high-frequency measurement may thus present a viable alternative GM monitoring method, providing higher confidence in GM investigation. In turn, this may provide sufficient confidence for regulators to permit well decommissioning with a low rate of methane leakage. Given the potential for methane biofiltration to further reduce atmospheric emissions (Stein and Hettiaratchi 2001; Reddy et al. 2014; Gunasekera et al. 2018), this could reduce the total number of idle wells and industry insolvency (Muehlenbachs, 2017). Financial and technical resources could also then be devoted to other more cost-effective emission reduction initiatives (Natural Resources Canada, 2019).

Conclusion

Inexpensive combustible gas concentration sensors were installed at several depths near to a case-study energy well with gas migration to collect a high-frequency time series of methane concentrations over a 19-day period. Results indicate several findings with potential application to enhance the understanding of GM detection and risk assessment practices:

1. Methane gas concentrations are generally higher at greater soil depths. A depth of only five cm below ground surface yielded order-of magnitude increases in measured concentrations compared to sensors at-grade with ground-surface.
2. Changes in methane concentrations observed after a moderate rain event indicate changes to the free phase gas migration pathways in the saturated or unsaturated zone.
3. Pronounced temporal variability in measured concentrations occurred over time scales of minutes to hours and days, with concentration changing by as much as four orders of magnitude over a few hours. More variation was observed at shallower depths and at-grade measurements (which are common practice) were most susceptible to temporal variation. Changing repeated snapshot

gas migration test results are expected when considering potential temporal variability at all depths.

4. Temporal variation in measured concentrations were correlated to wind speed, changing groundwater level, and barometric pressure.
5. GM detection success was generally high at this well. GM detection success was improved by using two measurement locations (in alignment with currently recommended practices), a lower detection limit, and greater measurement depth.
6. Repeated or long-term measurement may be necessary to observe concentration exceedances relevant for risk assessment.

These data will be useful to support policy development for GM detection, risk evaluation, and the end-of-life management of low-leaking energy wells that are not easily repaired.

Credit author statement

Cathy Ryan led funding acquisition and overall project direction and management. Neil Fleming led the study conceptualization, data acquisition and data analysis and wrote the initial draft. Tiago Morais assisted with data acquisition and data analysis and initial draft authorship. All authors contributed to editing and reviewing drafts.

Declaration of competing interests

The authors declare no competing personal or financial external interests that would have impacted the outcomes of this study.

Acknowledgments

This work was co-funded by the Alberta Upstream Petroleum Research Fund (AUPRF), administered by the Petroleum Technology Alliance of Canada (PTAC), and the Natural Science and Engineering Research Council of Canada (NSERC), Grant no. CRDPJ/503367-2016, with additional funding by the Canada First Research Excellence Fund (CFREF). We give thanks to the energy company that provided access to the study well and logistical support in field work. We also thank Chris Thompson and other members of the Well Integrity and Abandonment Society for their review of this work.

Author Biographies

Neil Fleming is a MSc student in Geoscience at the University of Calgary focusing on hydrogeology and field-scale gas migration studies. His research interests include field hydrogeology, and gas migration impacts on groundwater quality and atmospheric emissions. He is a gracious recipient of a 2019 SPE Canadian Educational Foundation scholarship.

Tiago Morais is a PhD student in Geoscience at the University of Calgary. Tiago's current research involves prediction and evaluation of environmental impacts potentially caused by unconventional oil and gas exploration and production. He received his MSc (2017) and BSc (2015) in Geoscience at the Federal University of Rio Grande do Sul, in Brazil.

Cathy Ryan is a Professor in Geoscience at the University of Calgary. She has authored more than 70 peer-reviewed research publications and also holds the method patent for a Passive Gas Diffusion Sampler. Dr. Ryan’s key areas of research include the fate and transport of free phase gases in the subsurface, groundwater-surface water interaction and water quality, and agricultural impacts on groundwater.

608

609 ## REFERENCES

610 Abbas, T. R., Abdul-Majeed, M. A., and Ghazi, I. N. 2010. Flow zones in unsaturated soil due to barometric
611 pumping. *Engineering and Technology Journal* **28**(10): 1900-1909.

612 Abbas, T. R. 2011. Effect of Water Table Fluctuation on Barometric Pumping in Soil Unsaturated Zone.
613 *Jordan Journal of Civil Engineering* **5** (4): 504-509. Jordan University of Science and Technology.

614 Alboiu, V. and Walker, T. R. 2019. Pollution, management, and mitigation of idle and orphaned oil and gas
615 wells in Alberta, Canada. *Environmental Monitoring and Assessment* **191**(10): 611.
616 https://doi.org/10.1007/s10661-019-7780-x

617 Abboud, J. M., Watson, T. L., and Ryan, M. C. 2020. Fugitive methane gas migration around Alberta's
618 petroleum wells. *Greenhouse Gases: Science and Technology* **11**(1), 37-51.
619 https://doi.org/10.1002/ghg.2029

620 Alberta Agriculture and Forestry, 2020. Alberta Climate Information Service (ACIS).
621 https://agriculture.alberta.ca/acis. (accessed October 2020)

622 Alberta Energy Regulator (AER). 2014. Directive 79: Surface Development in Proximity to Abandoned
623 Wells. Alberta, Canada. https://static.aer.ca/prd/2020-07/Directive079_0.pdf (accessed March
624 2021).

625 Alberta Energy Regulator (AER). 2021. Directive 20: Well Abandonment. Alberta, Canada.
626 https://static.aer.ca/prd/documents/directives/Directive020.pdf (accessed March 2021).

627 Anenberg, S. C., Schwartz, J., Shindell, D., et al. 2012. Global air quality and health co-benefits of mitigating
628 near-term climate change through methane and black carbon emission controls. *Environmental*
629 *Health Perspectives* **120**(6): 831-839. https://doi.org/10.1289/ehp.1104301

630 BC Oil and Gas Activities Act. 2020. Pipeline Crossing Regulation.
631 https://www.bclaws.ca/civix/document/id/complete/statreg/147_2012 (accessed October 2020).

632 Brandt, A.R., Heath, G.A., Kort, E.A., et al. 2014. Energy and environment methane leaks from North
633 American natural gas systems. *Science* **343**(6172): 733–735.
634 https://doi.org/10.1126/science.1247045.

635 British Colombia Oil and Gas Commission (BCOGC). 2019. Oil & Gas Operations Manual. Chapter 9 Well
636 Activity: Completion, Maintenance and Abandonment. Version 1.29.
637 https://www.bcogc.ca/node/13316/download (accessed August 2020).

638 Börjesson, G. and Svensson, B.H. 1997. Seasonal and diurnal methane emissions from a landfill and their
639 regulation by methane oxidation. *Waste Management & Research* **15**(1): 33-54.
640 https://doi.org/10.1177/0734242X9701500104.
641 Cahill, A., Steelman, C., Forde, O. et al. 2017. Mobility and persistence of methane in groundwater in a
642 controlled-release field experiment. *Nature Geoscience* **10**: 289-294.
643 https://doi.org/10.1038/ngeo2919.
644 Chamindu Deepagoda, T.K.K., Smits, K.M., and Oldenburg, C.M. 2016. Effect of subsurface soil moisture
645 variability and atmospheric conditions on methane gas migration in shallow subsurface.
646 *International Journal of Greenhouse Gas Control* **55**:105–117.
647 https://doi.org/10.1016/j.ijggc.2016.10.016.
648 Chamindu Deepagoda, T. K. K., Mitton, M., and Smits, K. 2018. Effect of varying atmospheric conditions on
649 methane boundary-layer development in a free flow domain interfaced with a porous media
650 domain. *Greenhouse Gases: Science and Technology* **8**(2): 335-348.
651 https://doi.org/10.1002/ghg.1743.
652 Dusseault, M. and Jackson, R. 2014. Seepage pathway assessment for natural gas to shallow groundwater
653 during well stimulation, in production, and after abandonment. *Environmental Geosciences* **21**(3):
654 107-126. https://doi.org/10.1306/eg.04231414004.
655 Dusseault, M. B., Jackson, R. E., and Macdonald, D. 2014. Towards a road map for mitigating the rates and
656 occurrences of long-term wellbore leakage. Special Report. University of Waterloo and Geofirma
657 Engineering. https://geofirma.com/wp-content/uploads/2015/05/lwp-final-
658 report_compressed.pdf
659 Engelder, T. and Zevenbergen, J. 2018. Analysis of a gas explosion in Dimock PA (USA) during fracking
660 operations in the Marcellus gas shale. *Process Safety and Environmental Protection*. **117**: 61-66.
661 https://doi.org/10.1016/j.psep.2018.04.004.
662 Erno, B. and Schmitz, R. 1996. Measurements of soil gas migration around oil and gas wells in the
663 Lloydminster area. *Journal of Canadian Petroleum Technology* **35**(07). PETSOC-96-07-05.
664 https://doi.org/10.2118/96-07-05.
665 Fleming, N., Morais, T., Kennedy, C. et al. 2019. Evaluation of SCVF and GM measurement approaches to
666 detect fugitive gas migration around energy wells. Presented at Geoconvention 2019. Calgary,
667 Canada. 13-17 May 2019.

668 Fleming, N. Morais, T. Mayer, K.U. Ryan, M.C. 2021. Spatiotemporal variability of fugitive gas migration
669 emissions around a petroleum well. *Atmospheric Pollution Research* **12**(06).
670 https://doi.org/10.1016/j.apr.2021.101094
671 Forde, O. N., Cahill, A. G., Beckie, R. D. et al. 2019a. Barometric-pumping controls fugitive gas emissions
672 from a vadose zone natural gas release. *Scientific Reports* **9**(1): 1-9.
673 https://doi.org/10.1038/s41598-019-50426-3.
674 Forde, O.N., Mayer, K.U., Cahill, A.G., et al. 2018. Vadose zone gas migration and surface effluxes after a
675 controlled natural gas release into an unconfined shallow aquifer. *Vadose Zone Journal* **17**:1-16.
676 https://doi.org/10.2136/vzj2018.02.0033.
677 Forde, O. N., Mayer, K. U., and Hunkeler, D. 2019b. Identification, spatial extent and distribution of fugitive
678 gas migration on the well pad scale. *Science of the Total Environment* **652**: 356-366.
679 https://doi.org/10.1016/j.scitotenv.2018.10.217.
680 Fukui, M. 1987. Soil water effects on concentration profiles and variations of 222Rn in a vadose
681 zone. *Health Physics* **53**(2): 181-186.
682 Gorody, A. W. 2012. Factors affecting the variability of stray gas concentration and composition in
683 groundwater. *Environmental Geosciences* **19**(1): 17-31. https://doi.org/10.1306/eg.12081111013.
684 Government of Saskatchewan. 2015. Gas Migration, Guideline PNG026. The Oil and Gas Conservation
685 Regulations, 2012. https://pubsaskdev.blob.core.windows.net/pubsask-prod/84462/84462-
686 Guideline_PNG026_Gas_Migration.pdf
687 Gunasekera, S. S., Hettiaratchi, J. P., Bartholameuz, E. M. et al. 2018. A comparative evaluation of the
688 performance of full-scale high-rate methane biofilter (HMBF) systems and flow-through
689 laboratory columns. *Environmental Science and Pollution Research* **25**(36): 35845-35854.
690 https://doi.org/10.1007/s11356-018-3100-1.
691 Gurevich, A. E., Endres, B. L., Robertson Jr, J. O., et al. 1993. Gas migration from oil and gas fields and
692 associated hazards. *Journal of Petroleum Science and Engineering* **9**(3): 223-238.
693 https://doi.org/10.1016/0920-4105(93)90016-8.
694 Health Canada. 2019. Guidelines for Canadian Drinking Water Quality—Summary Table. Water and Air
695 Quality Bureau, Healthy Environments and Consumer Safety Branch, Health Canada, Ottawa,
696 Ontario. https://www.canada.ca/content/dam/hc-sc/migration/hc-sc/ewh-
697 semt/alt_formats/pdf/pubs/water-eau/sum_guide-res_recom/sum_guide-res_recom-eng.pdf
698 (accessed March 2021).

699 Henan Hanwei Electronics Co. Ltd. MQ-4 Semiconductor Sensor for Natural Gas.
700 https://www.pololu.com/file/0J311/MQ4.pdf (accessed August 2020).
701 Honeycutt, W. T., Ley, M. T., and Materer, N. F. 2019. Precision and limits of detection for selected
702 commercially available, low-cost carbon dioxide and methane gas sensors. *Sensors* **19**(14): 3157.
703 https://doi.org/10.3390/s19143157.
704 IPCC. 2013. Climate Change 2013: The Physical Science Basis. Contribution of Working Group I to the Fifth
705 Assessment Report of the Intergovernmental Panel on Climate Change [Stocker, T.F. D., Qin, G.-K.,
706 Plattner, M., et al.]. Cambridge University Press, Cambridge, United Kingdom and New York, NY,
707 USA, 1535 pp.
708 Kang, M., Kanno, C. M., Reid, M. C. et al. 2014. Direct Measurements of Methane Emissions from
709 Abandoned Oil and Gas Wells in Pennsylvania. Proc Natl Acad Sci **111** (51): 18173–18177.
710 https://doi.org/10.1073/pnas.1408315111.
711 Kuang, X., Jiao, J. J., and Li, H. 2013. Review on airflow in unsaturated zones induced by natural
712 forcings. *Water Resources Research* **49**(10): 6137-6165. https://doi.org/10.1002/wrcr.20416.
713 Lyman, S. N., Tran, H. N., Mansfield, M. L. et al. 2020. Strong temporal variability in methane effluxes from
714 natural gas well pad soils. *Atmospheric Pollution Research* **11**(8):1386-1395.
715 https://doi.org/10.1016/j.apr.2020.05.011.
716 Mitton, M. 2018. *Subsurface methane migration from natural gas distribution pipelines as affected by soil*
717 *heterogeneity: field scale experimental and numerical study*. Doctoral dissertation, Colorado School
718 of Mines. Arthur Lakes Library.
719 https://mines.primo.exlibrisgroup.com/permalink/01COLSCHL_INST/1i00sit/alma99758270290234
720 1.
721 Molofsky, L. J., Connor, J. A., Van De Ven, C. J., et al. 2021. A Review of Physical, Chemical, and
722 Hydrogeologic Characteristics of Stray Gas Migration: Implications for Investigation and
723 Remediation. *Science of The Total Environment* 146234.
724 https://doi.org/10.1016/j.scitotenv.2021.146234.
725 Muehlenbachs, L. 2017. 80,000 inactive oil wells: A blessing or a curse? The School of Public Policy,
726 University of Calgary, Alberta, Canada. *SPP Briefing Paper* **10**(3). https://www.policyschool.ca/wp-
727 content/uploads/2017/03/Inactive-Oil-Wells-Muehlenbachs-1.pdf.
728 Nachshon, U., Weisbrod, N., Dragila, M. I. et al. 2011. The Importance of Advective Fluxes to Gas Transport
729 Across the Earth-Atmosphere Interface: The Role of Thermal Convection. In Planet Earth 2011-
730 Global Warming Challenges and Opportunities for Policy and Practice. IntechOpen.

731 Natural Resources Canada. 2019. Technology roadmap to improve wellbore integrity: summary report.
732 https://www.nrcan.gc.ca/sites/www.nrcan.gc.ca/files/pdf/NRCan_Wellbore_e_WEB(1)%20(1).pdf
733 Noomen, M. F., Van der Werff, H. M. and Van der Meer, F. D. 2012. Spectral and spatial indicators of
734 botanical changes caused by long-term hydrocarbon seepage. *Ecological Informatics* **8**: 55-64.
735 https://doi.org/10.1016/j.ecoinf.2012.01.001.
736 Occupational Health and Safety Code. 2009. Part 10: Fire and Explosion Hazards. Alberta, Canada.
737 https://open.alberta.ca/dataset/757fed78-8793-40bb-a920-6f000853172b/resource/c8f462b7-
738 e8c3-4c4a-a5b3-c055648c61ee/download/4403880-part-10-fire-and-explosion-hazards.pdf
739 (accessed March 2021).
740 Oliveira, S., Viveiros, F., Silva, C. et al. 2018. Automatic Filtering of Soil CO2 Flux Data; Different Statistical
741 Approaches Applied to Long Time Series. *Frontiers in Earth Science* **6**: 208.
742 https://doi.org/10.3389/feart.2018.00208
743 Office of the Regulator of Oil and Gas Operations (OROGO). 2017. Well Suspension and Abandonment
744 Guidelines. Northwest Territories Oil and Gas Operations Act.
745 https://www.orogo.gov.nt.ca/sites/orogo/files/resources/orogo_well_suspension_and_abandonme
746 nt_guidelines_and_interpretation_notes.pdf#page=24&zoom=100,92,96 (accessed March 2021).
747 Poulsen, T. G., Pourber, A., Furman, A. et al. 2017. Relating wind-induced gas exchange to near-surface
748 wind speed characteristics in porous media. *Vadose Zone Journal* **16**(8): 1-13.
749 https://doi.org/10.2136/vzj2017.02.0039.
750 Pretch, P. and Dempster, D. 2017. Newfoundland & Labrador Basis for Development of Guidance Related
751 to Hydraulic Fracturing: Part 3.
752 http://www.nr.gov.nl.ca/nr/energy/pdf/nl_hydraulic_fracturing_pt3_appendix.pdf (accessed March
753 2021).
754 Province of Alberta. 2020. Pipeline Act. https://www.qp.alberta.ca/documents/Acts/p15.pdf (accessed
755 March 2021).
756 R Core Team. 2020. R: A language and environment for statistical computing. R Foundation for Statistical
757 Computing, Vienna, Austria. https://www.R-project.org/ (Accessed October 2020).
758 Reddy, K. R., Yargicoglu, E. N., Yue, D., et al. 2014. Enhanced microbial methane oxidation in landfill cover
759 soil amended with biochar. *Journal of Geotechnical and Geoenvironmental Engineering* **140**(9):
760 04014047. https://doi.org/10.1061/(ASCE)GT.1943-5606.0001148.

761 Redeker, K.R., Baird, A.J., and The, Y. A. 2015. Quantifying wind and pressure effects on trace gas fluxes
762 across the soil-atmosphere interface. *Biogeosciences* **12**(24):7423–7434.
763 https://doi.org/10.5194/bg-12-7423-2015.
764 Riddick, S. N., Mauzerall, D. L., Celia, M. A., et al. 2020. Variability observed over time in methane emissions
765 from abandoned oil and gas wells. *International Journal of Greenhouse Gas Control* **100**: 103116.
766 https://doi.org/10.1016/j.ijggc.2020.103116.
767 Saint-Vincent, P. M., Reeder, M. D., Sams III, J. I., et al. 2020. An analysis of abandoned oil well
768 characteristics affecting methane emissions estimates in the Cherokee Platform in Eastern
769 Oklahoma. *Geophysical Research Letters* **47:**(23). https://doi.org/10.1029/2020GL089663.
770 Sandl, E., Cahill, A. G., Welch, L., et al. 2021. Characterizing oil and gas wells with fugitive gas migration
771 through Bayesian multilevel logistic regression. *Science of The Total Environment* **769:** 144678.
772 https://doi.org/10.1016/j.scitotenv.2020.144678.
773 Schiffner, D., Kecinski, M., and Mohapatra, S. 2021. An updated look at petroleum well leaks, ineffective
774 policies and the social cost of methane in Canada's largest oil-producing province. *Climatic*
775 *Change* **164**(3): 1-18. https://doi.org/10.1007/s10584-021-03044-w.
776 Schout, G., Griffioen, J., Hassanizadeh, S. M. et al. 2019. Occurrence and fate of methane leakage from cut
777 and buried abandoned gas wells in the Netherlands. *Science of the Total Environment* **659:** 773-
778 782. https://doi.org/10.1016/j.scitotenv.2018.12.339.
779 Sekhar, P. K., Kysar, J., Brosha, E. L. et al. 2016. Development and testing of an electrochemical methane
780 sensor. *Sensors and Actuators B: Chemical* **228:** 162-167. https://doi.org/10.1016/j.snb.2015.12.100
781 Simpson, I. J., Edwards, G. C., and Thurtell, G. W. 1999. Variations in methane and nitrous oxide mixing
782 ratios at the southern boundary of a Canadian boreal forest. *Atmospheric Environment* **33**(7):
783 1141-1150. https://doi.org/10.1016/S1352-2310(98)00235-0.
784 Statutes of Saskatchewan. 1998. The Pipeline Act. https://www.canlii.org/en/sk/laws/stat/ss-1998-c-p-
785 12.1/latest/part-1/ss-1998-c-p-12.1-part-1.pdf (accessed March 2021).
786 Stein, V. B. and Hettiaratchi, J. P. A. 2001. Methane oxidation in three Alberta soils: influence of soil
787 parameters and methane flux rates. *Environmental Technology* **22**(1): 101-111.
788 https://doi.org/10.1080/09593332208618315.
789 Szatkowski, B., Whittaker, S., and Johnston, B. 2002. Identifying the source of migrating gases in surface
790 casing vents and soils using stable Carbon Isotopes, Golden Lake Pool, West-central
791 Saskatchewan. Summary of Investigations, vol 1 Saskatchewan Geological Survey, Regina, SK,
792 Canada.

Trudel, E., Bizhani, M., Zare, M. et al. 2019. Plug and abandonment practices and trends: A British Columbia perspective. *Journal of Petroleum Science and Engineering* **183**: 106417. https://doi.org/10.1016/j.petrol.2019.106417.

Ulrich, B. A., Mitton, M., Lachenmeyer, E. et al. 2019. Natural gas emissions from underground pipelines and implications for leak detection. *Environmental Science and Technology Letters* **6**(7): 401-406. https://doi.org/10.1021/acs.estlett.9b00291.

Van De Ven, C. J., Abraham, J. E., and Mumford, K. G. 2020. Laboratory investigation of free-phase stray gas migration in shallow aquifers using modified light transmission. *Advances in Water Resources* **139**: 103543. https://doi.org/10.1016/j.advwatres.2020.103543

Vidic, R., Brantley, S., Vandenbossche, J., et al. 2013. Impact of shale gas development on regional water quality. *Science* **340**(6134). https://doi.org/10.1126/science.1235009.

Zavala-Araiza, D., Lyon, D. R., Alvarez, R. A., et al. 2015. Reconciling divergent estimates of oil and gas methane emissions. *Proceedings of the National Academy of Science* **112**(51): 15597-15602. https://doi.org/10.1073/pnas.1522126112.

Appendix A—Sensor Description and Field Installation

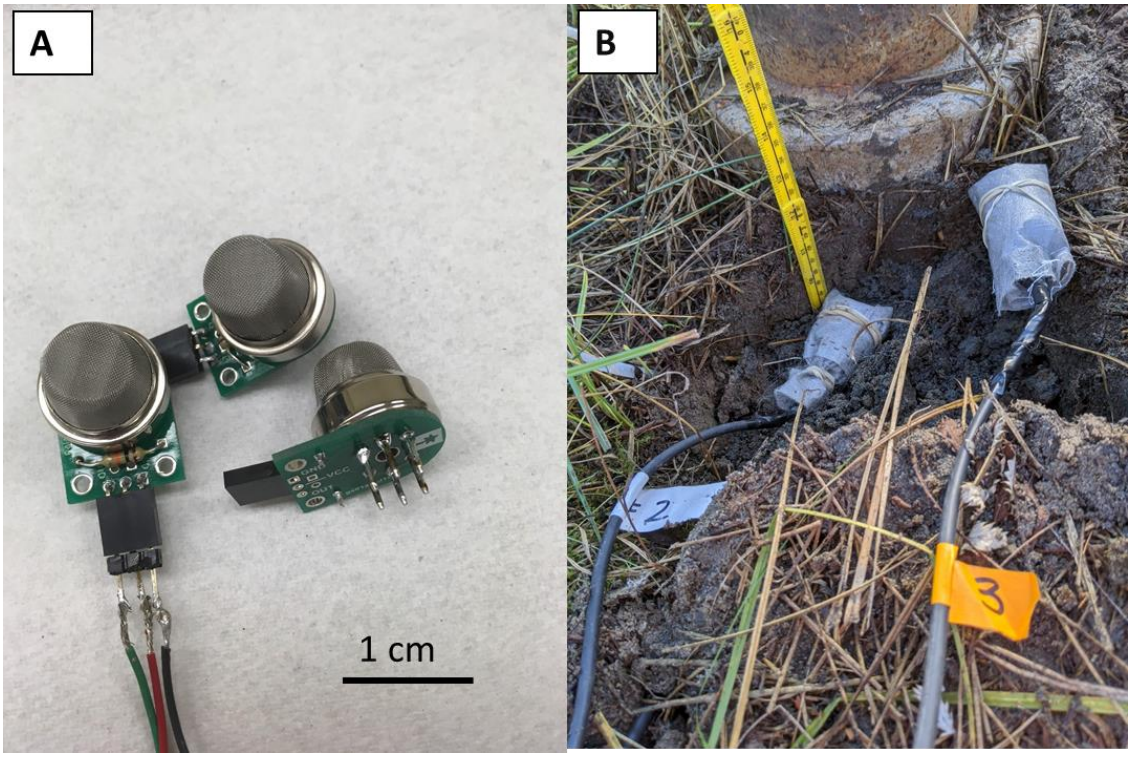

Fig. A-1—A) Photograph of MQ-4 sensors wired to commercially available circuit board with 10 000 Ω resistor. B) Field-installation of sensors at the 5 cm and 0 cm depth next to outermost well casing. (Soil later backfilled to grade.)

Two nests of MQ4 chemoresistive gas sensors were installed near the well casing, with sensors at 0, 5, and 30 cm depths. The sensors within the nests were horizontally offset to limit vertical preferential gas flow, while maintaining a radial distance from the outermost well casing of approximately five centimeters. The sensor housings were centered on the described depth, such that '0 cm depth' sensor was partially buried at ground surface. Two additional control sensors were installed five meters west of the wellhead, both at 5 cm below ground surface with one sensor in native soil and one sensor enclosed within a plastic container (0.3 m diameter by 0.3 m depth) filled with moist sand to isolate the sensor from subsurface gases while allowing exchange with atmospheric gases and heat. The sensors were mounted on a commercially available circuit board with a three-wire output, then enclosed within a perforated plastic 40 mL bottle wrapped in geotextile to exclude sediment from direct contact with the sensor and installed in an orientation that would shield the sensors from downward water drainage (Fig. A-1). A common external five-volt DC power supply ensured adequate current for the sensor heating loops, with estimated

continuous per-sensor requirements of ≤900mW (Henan Hanwei Electronics Co. Ltd). The continuous power supply was provided by an overpowered on-site photovoltaic system with 6 X 300 W solar panels charging an 1800 Ah battery bank outputting steady 120V AC power through a 4000 W inverter, which then powered the 12 VDC and 5 VDC power adapters for the datalogger and heating loops, respectively. (Estimated total continuous system power demands for the 8 sensors was less than 30 W).

Single-ended analog circuit voltages (mV) were sampled from the sensor circuit every minute and recorded on a datalogger (CR1000, Campbell Scientific) over a period of 20 days. The first 24 hours of the data series was discarded, following the recommended 'burn-in' time for full heating of the sensor (Henan Hanwei Electronics Co. Ltd.; Honeycutt et al. 2019).

Appendix B—Sensor Calibration

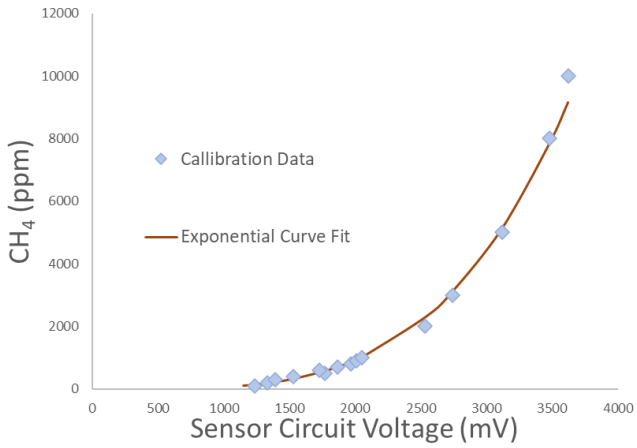

Fig. B-1—Example exponential curve fit to calibration data for sensor #8.

While the manufacturer provides empirically derived formulae for converting the sensor output to a combustible gas concentration estimates, an independent calibration was preferred to fully account for the non-linear sensor-specific response to increasing voltages across the wide range of encountered methane gas concentrations (Henan Hanwei Electronics Co. Ltd.; Riddick et al. 2020). Sensors were lab calibrated to determine the non-linear response between sensor circuit voltage and methane concentrations **(Fig. B-1).** Calibration procedure involved injecting progressively greater volumes of pure CH_4 gas into an enclosed vessel containing all 8 sensors and registering the sensor response at each step. The vessel was vented between injections, allowing the sensors to stabilize to background values. The

sensor circuit response was manually averaged at stable values to exclude the sensor overshoot peak (Honeycutt et al. 2019). These data of sensor circuit voltage and CH_4 concentration (obtained through calculation of injected gas volume in comparison to the vessel volume) were fitted to an exponential-type curve by varying the parameters c, E, and b to optimize the least sum of squared deviations using MS Excel's 'Solver' function, yielding a calibration curve specific to each sensor **(Eq.1; Table B-1)**.

$$[CH_4]_{pppm.estimated} = c * E^{Raw.Voltage*b} + k \quad \text{..... (1)}$$

The exponential curves were then adjusted with a constant k to output 2 ppm CH_4 as the free-air background concentration for the mean sensor circuit voltage obtained in the field at the end of the measurement period when all sensors were placed exposed to fresh air 50 m upwind from the well. While the sensors response is known to vary slightly depending on relative humidity and temperature, no corrections were made for these parameters (Honeycutt et al. 2014). Previous field measurements by other authors have shown a good agreement between MQ4 measurements and concentrations measured from gas samples analyzed with gas chromatography (Riddick et al. 2020). This gives greater confidence in the capability of the MQ4 sensor to distinguish between the responses closer to the well compared to the lower concentrations further away. No gas sampling or additional concentration measurements were performed during this field experiment. While this did avoid perturbing in-soil gas movement, it was not possible to validate the MQ4 sensor concentrations against another measured value.

Sensor	**1**	**2**	**3**	**4**	**5**	**6**	**7**	**8**
Coeff c	0.022	0.776	0.260	0.186	0.421	0.140	25.933	43.956
Coeff b	0.0026	0.0021	0.0026	0.0027	0.0026	0.0027	0.0020	0.0015
Exponent	3.1437	2.9540	2.5257	2.7066	2.4722	2.5604	2.2504	2.6591
Constant (k)	1.7	-4.1	0.2	-219.0	-1.3	0.5	-86.6	-188.3
R^2	0.970	0.971	0.993	0.951	0.989	0.992	0.998	0.994
Field Installation Location (Distance from Well, Depth in Soil Below Ground Surface)	30 cm, West	5 cm, West	0 cm, West	5 m West, 5 cm Native Soil	5 m West, 5 cm Isolated Sand	30 cm, East	5 cm, East	0 cm, East

Table B-1—Calibration curve parameters and description of sensor field installation location as depth below ground surface and side of well casing

Appendix C—Baseline Noise and Sensor Response Tests

Since all sensors were using a common external five-volt source for the sensing and heating loop, independent sensor response was verified by individually subjecting each sensor to a high concentration of combustible gas and ensuring that the voltage output of other sensors were not affected (Fig. C-1).

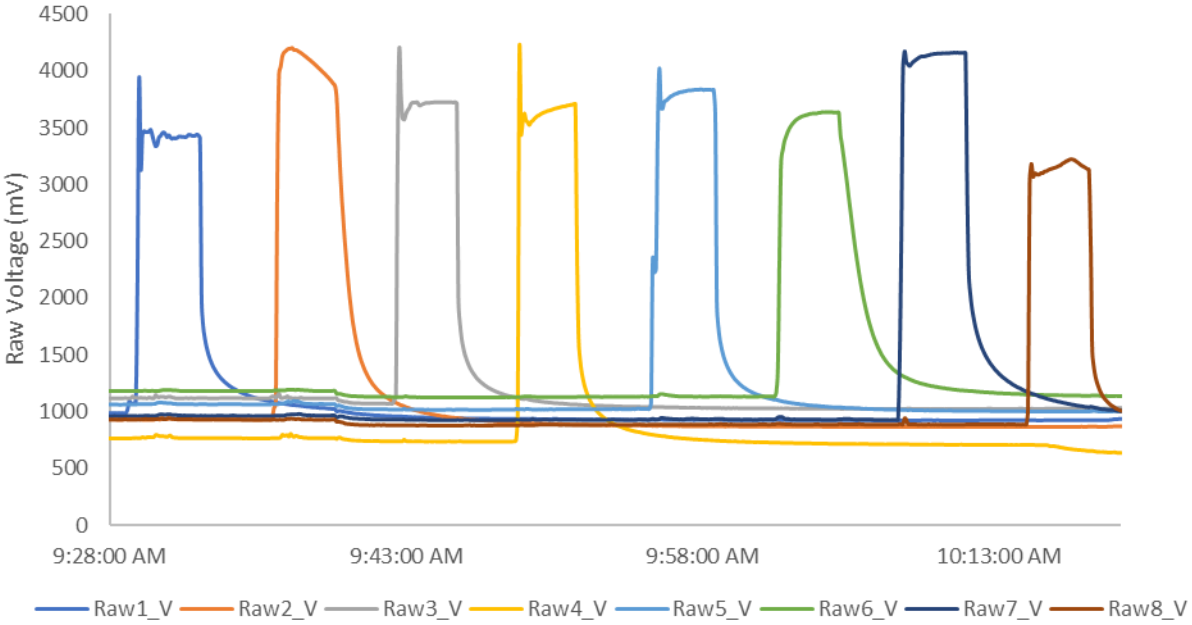

Fig. C-1—Independent sensor response showing unchanged sensor circuit voltages on other sensors while individually subjecting sensors to elevated methane gas concentrations

A baseline noise test then sought to determine the expected degree of variation in sensor response that might be expected during normal operation in atmospheric air (after Honeycutt et al. 2014). The sensors measured atmospheric concentration responses in an open laboratory setting every 15 seconds for several days, after which the sensing voltage was converted to ppm CH_4 using the field-adjusted calibration parameters (Table C-1). Variance is displayed graphically and represented through the coefficient of variation, CV

$$CV = \frac{\sigma}{\mu}$$

Where σ is the standard deviation of measurement, and μ is the mean calibrated sensor response in ppm CH_4.

			Coefficient of Variation				
			Lab		Field		
Sensor #	Field Location	Field Depth	Full Period	Shaded Stable Period	Full Series	Mean of all 12 h periods	Mean of all 1 h periods
		-- cm --	---------- % ----------				
1	West along casing	30	2.0	0.6	113.3	49.9	11.0
2		5	10.4	3.7	169.4	73.7	47.2
3		0	7.7	2.0	148.7	89.7	52.1
6	East along casing	30	8.8	1.3	57.1	15.8	5.9
7		5	12.4	4.3	71.5	12.9	5.1
8		0	79.1	88.6	97.7	31.4	9.4
4	5 m Distal	5 (baseline)	0.1	0.0	77.2	4.8	1.0
5		5 (isolated)	8.9	1.8	20.5	4.0	3.7

Table C-1—Coefficient of variation (normalised standard deviation of measurement) in % for lab baseline noise tests and field data, demonstrating the variability in measured values as ppm CH_4. Field locations correspond to the direction on the side of the well casing as West (W) or East (E) and depth in-soil (30 cm, 5 cm, or 0 cm). The "5 (isolated)" sensor was 5 m east of the well at 5 cm depth and isolated from soil gases.

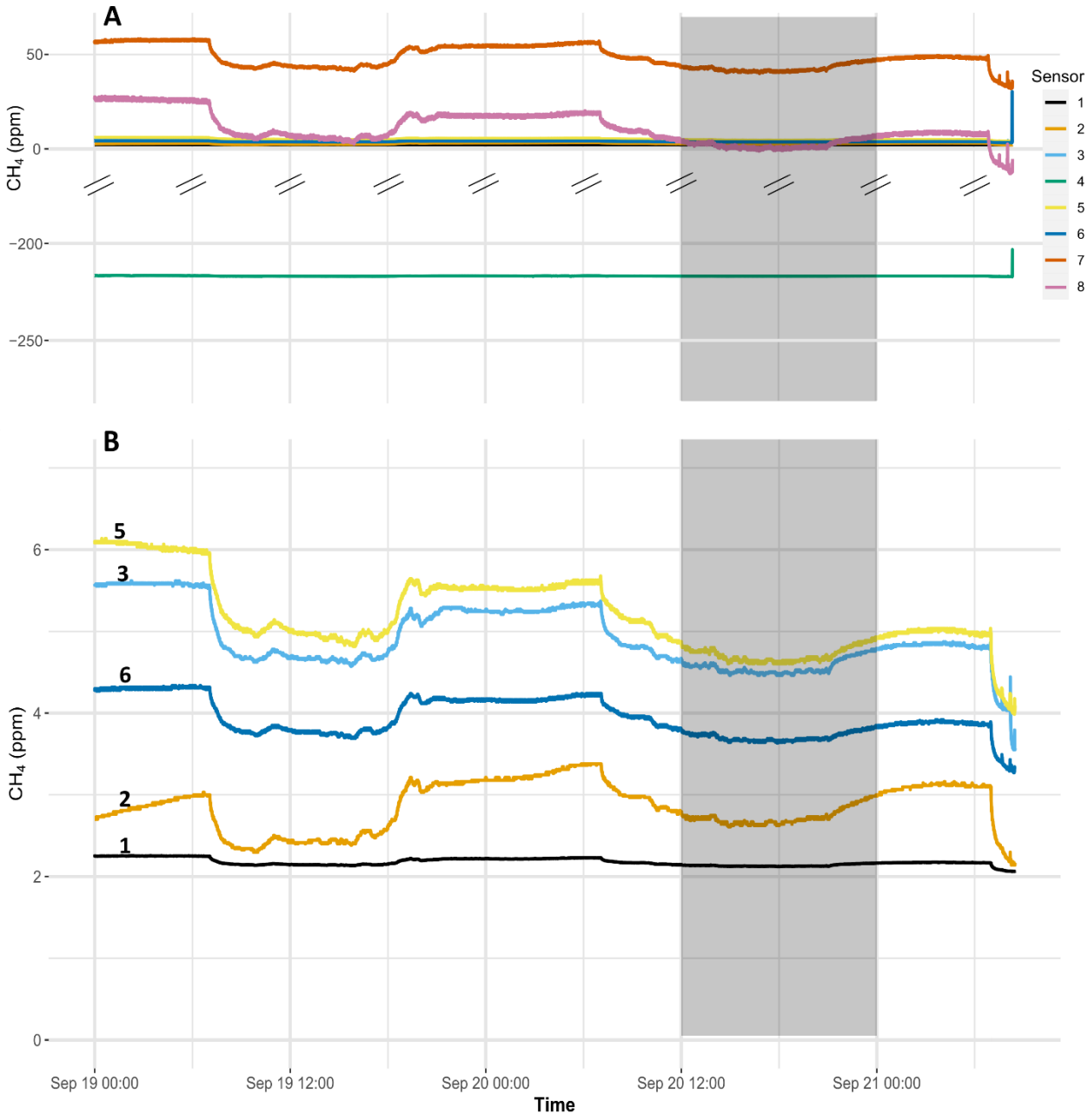

Fig. C-2—Lab baseline noise test showing sensor response as calibrated ppm CH_4 for 15 second frequency measurements over > two days. A) shows all sensors (note Y scale break), while B) shows a close-up of 5 selected sensors, with concentrations close to expected atmospheric values, labelled by sensor number. Shaded region corresponds to a 12-hour selected 'Shaded Stable Period' shown in Table C-1.

Appendix D—Supplementary Field Data and Discussion

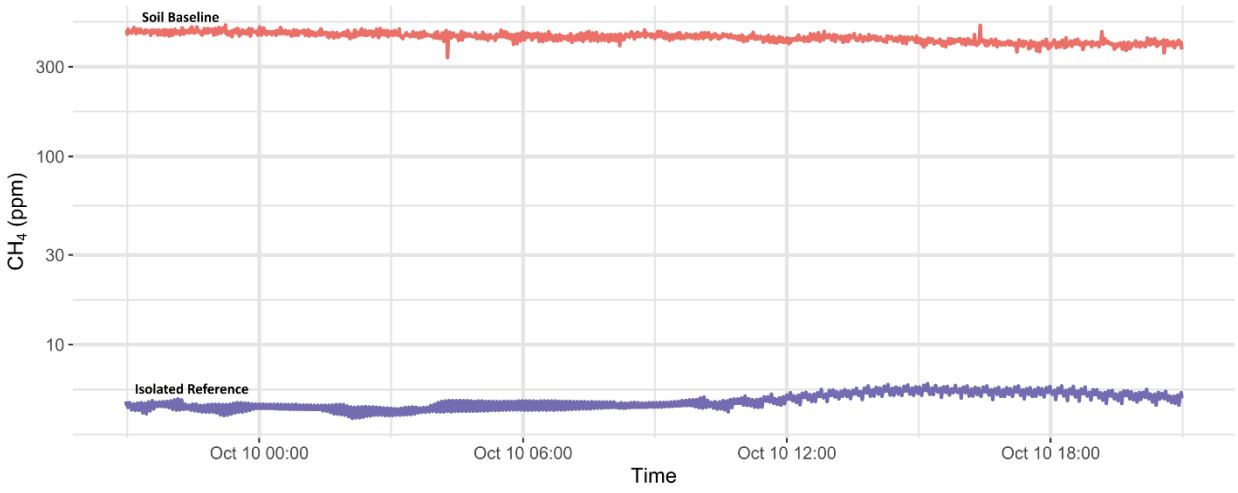

Fig. D-1—Time series one-minute frequency combustible soil gas concentrations (log ppm CH_4) over 48 hours at 0.05 m depth and 5 m East of the energy well casing. The 'Soil Baseline' sensor is installed in native soil, while the 'Isolated Reference' sensor is excluded from site soil gases.

The 'Isolated Reference' sensor still displays some moderate variability, both on a pronounced daily cycle (Fig. 5) and as short-term variation (Fig. D-1). It is expected that all sensors will exhibit some amount of noise and varying sensor response due to changing sensor temperatures and relative humidity. Ideal sensing relative humidity below 65% may have been exceeded in the soil (Henan Hanwei Electronics Co. Ltd.) A lack of gas samples or additional field measurements precluded direct verification of the MQ4 CH_4 concentrations in field temperature and humidity conditions, and there may have been small changes impacting the accuracy of the (laboratory derived) calibration curves in the field conditions. However, the short-term and daily variations for the distal sensors were relatively minor (e.g., resulting in calibrated sensor responses ranging between 0-10 ppm for the 'Isolated Reference' sensor), despite changing weather conditions and temperatures ranging over 30 ℃. There was a much larger range in sensor response for the sensors adjacent to the well casing, despite exposure to similar variations in temperature and humidity. Therefore, the relatively small variation in the two distal sensors, and especially for the 'Isolated Reference', indicates that a large variation in sensor response in the nests around the well casing is best explained by changing soil gas concentrations as opposed to other gas-concentration independent factors such as temperature, humidity, or sensor noise.

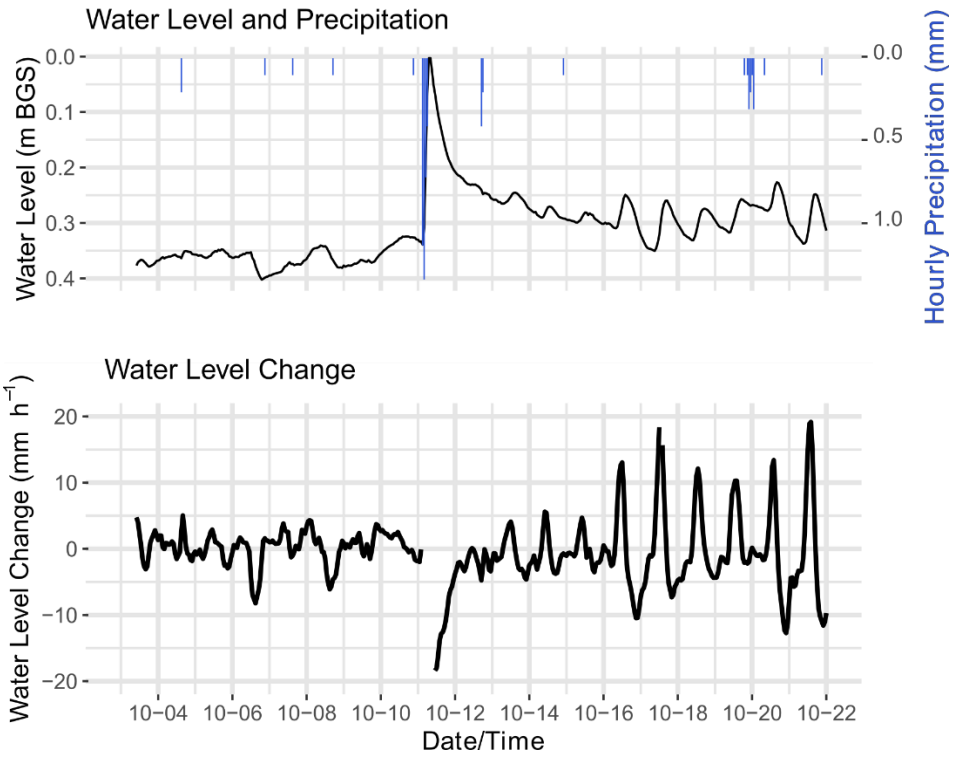

924

925 **Fig. D-2—**Measured site water level in a piezometer 1.25 m south of well-centre and 1.0 m below ground
926 surface (BGS), and precipitation at the nearest weather station. Water level change rate excludes a large
927 change occurring at the time of the cumulative 3.5 mm precipitation event on Oct. 11, 2020.

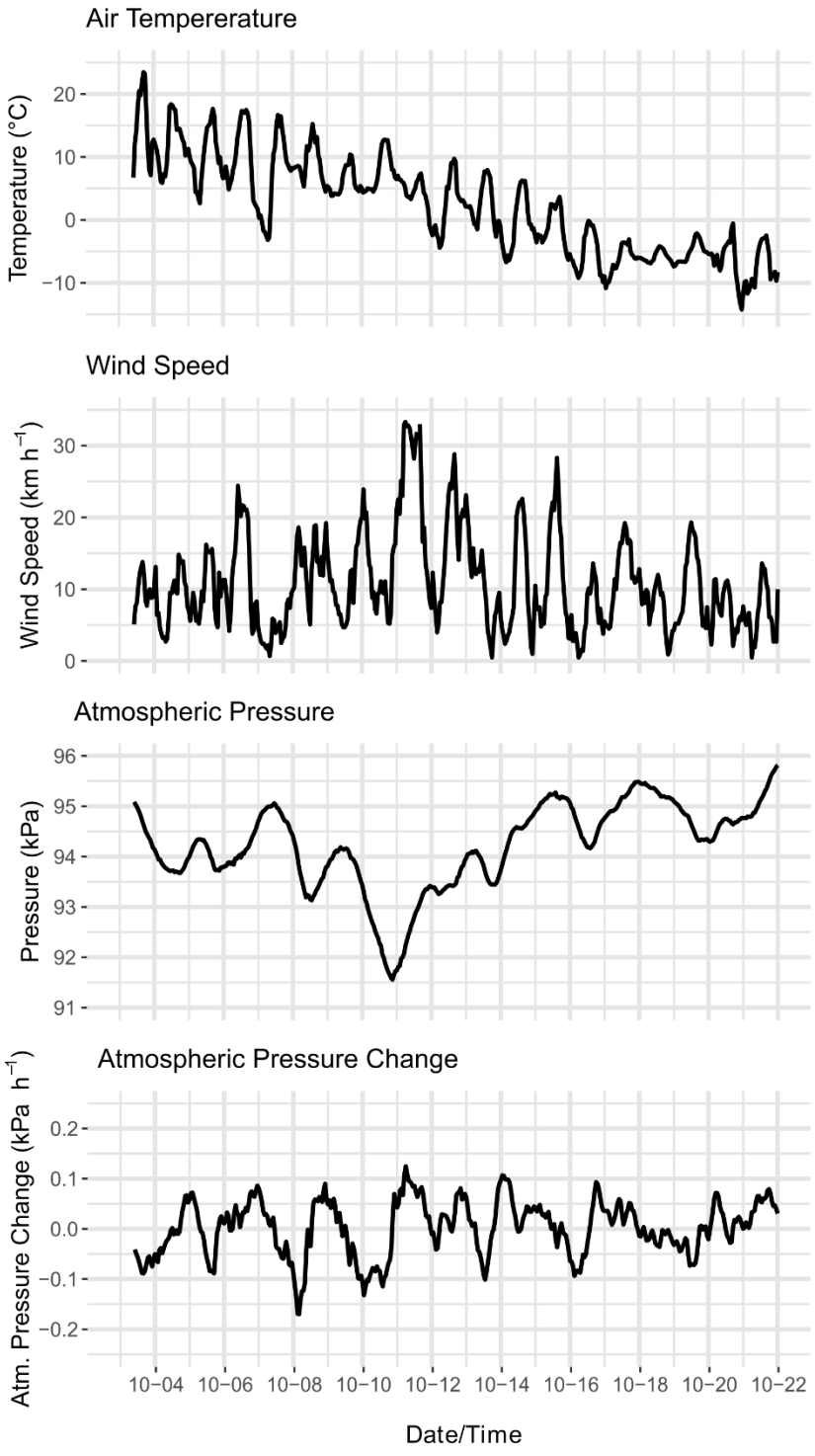

928

929 **Fig. D-3—**Meteorological factors considered in regression analysis with measured soil gas concentrations.

930